Journal of Medicinal Chemistry

Article

Developing Anticancer Ferric Pro-drugs Based on the N-donor Residues of Human Serum Albumin Carrier IIA Subdomain

Jinxu Qi, Yi Gou, Yao Zhang, Kun Yang, Shifang Chen, Li Liu, Xiaoyang Wu, Tao Wang, Wei Zhang, and Feng Yang

J. Med. Chem., **Just Accepted Manuscript** • DOI: 10.1021/acs.jmedchem.6b00509 • Publication Date (Web): 21 Jul 2016

Just Accepted

ACS Publications

Journal of Medicinal Chemistry is published by the American Chemical Society. 1155 Sixteenth Street N.W., Washington, DC 20036

Developing Anticancer Ferric Pro-drugs Based on the N-donor Residues of Human Serum Albumin Carrier IIA Subdomain

Jinxu Qi[1], Yi Gou[1], Yao Zhang[1], Kun Yang[1], Shifang Chen[1], Li Liu[2], Xiaoyang Wu[3], Tao Wang[2]*, Wei Zhang[1]*, Feng Yang[1]*

[1] School of pharmacy, Nantong University, Nantong, Jiangsu, China.

[2] Department of Biology, Southern University of Science and Technology, Shenzhen, Guangdong, China.

[3] Ben May Department for Cancer Research, University of Chicago, Chicago, IL, USA.

*Corresponding author: Feng Yang

Email : fyang@mailbox.gxnu.edu.cn

Phone/Fax : 86-773-584-8836

Address: 9 Seyuan Road, Nantong, Jiangsu, China. Zip code: 226019

KEYWORDS: human serum albumin; ferric compound; anticancer mechanism; tumor targeting; therapeutic effect.

Abstract

To improve the selectivity, delivery and activity of ferric (Fe) anticancer agents, we design pro-drugs based on N-donor residues of the human serum albumin (HSA) carrier IIA subdomain. We synthesized six Fe(III) compounds derived from 2-Hydroxy-1-naphthaldehyde thiosemicarbazone (**7**-**12**). HSA complex structure revealed that Fe compound binds to the hydrophobic cavity in the HSA IIA subdomain. Lys199 and His242 of HSA replace the two Cl atoms of Fe compound, coordinating with Fe^{3+}. *In vivo* data revealed that compound **12** and HSA-**12** complex inhibit the growth of the liver tumor, and the HSA-**12** complex has stronger targeting ability and therapeutic efficacy than compound **12** alone. In addition, our results have shown that compound **12** and HSA-**12** complex induce Bel-7402 cell death possible by several mechanisms.

Introduction

Many studies have shown that metal compounds have a biological and chemical diversity that organic drugs simply do not.[1,2] Certain metal-organic ligand complexes have increased biological activity over ligands alone, especially in antitumor activity.[3,4] Therefore, a different strategy for developing anticancer drugs would be to design and synthesize metal complexes derived from organic ligands.[5-7]

Current studies reveal that Fe and Cu chelators are promising novel anticancer agents, as cancer cells can absorb more Fe and Cu than the normal cells.[8,9] For example, both desferrioxamine (DFO) (through *in vitro* and *in vivo* studies) and 2-hydroxy-1-naphthylaldehyde isonicotinoyl have limited tumor activity.[10-12] In fact, 3-aminopyridine-2-carboxaldehyde thiosemicarbazone (3-AP) has reached clinical trials as an anticancer therapeutic.[12] In addition, a series of novel chelators, such as thiosemicarbazones, have pronounced anticancer activity and selectivity, and overcome resistance to established chemotherapeutics *in vivo*.[8,9] However, these chelators may produce low antitumor activity; in addition, dose-limiting side effects, including methemoglobinemia and hypoxia, have limited their potential in the clinic.[12-14] Richardson et al. have investigated the effects of Cu(II) complexes with thiosemicarbazones and determined that they have the potential for antipoliferative activity along with redox in an accessible range for natural reductants.[3,12] These pioneering studies have shown novel anticancer metal agents, derived from thiosemicarbazone ligands can be developed.[2] Currently, metal compounds derived with a great variety of ligands are under extensive investigation as anticancer

agents.[15,16]

Although a large number of metal compounds have been evaluated *in vitro* and *in vivo,* and some have even reached clinical trials, researchers still need to determine how to increase targeting success and decrease *in vivo* side effects;[2] the use of pro-drugs and drug carriers may help to tackle these issues.[17-20] Human serum albumin (HSA) is a promising non-toxic, non-antigenic, biocompatible, and biodegradable endogenous protein drug delivery system that lacks immunogenicity.[21-24] HSA, the most abundant protein in plasma with many active residues, can bind to a diverse group of exogenous compounds.[25-28] Therefore, to improve the targeting of anticancer agents, these properties can be utilized to design novel anticancer pro-drugs.[20,30] There are two major ways for design pro-drugs based on HSA: through chemically coupling the metal pro-drug to the residues of HSA; or through direct complexation of the pro-drug with HSA.[30,31] Unfortunately, there can be problems with the release of a drug when metal compounds are delivered to cancer cells using complexed HSA carriers *in vivo* due to the strength of the binding between HSA and the pro-drug.[30] For example, the metal pro-drug can be released from HSA prematurely if it is not bound strongly or it may not be released at all if the bond is too tight. To address these issues, Yang et al. proposed the use of a metal pro-drug whose design is based on the natural HSA IIA subdomain and the known cancer cell.[30,32-34] The metal pro-drug can contain potential leaving group(s) with no anti-cancer activity that are then displaced by Lys199 and/or His242 residue(s) of HSA. This is outlined below.

Among the next generation of metal-based anticancer compounds, Fe anticancer compounds may be promising.[1] In humans, Fe is an essential bioactive element with an oxidative nature. HSA has active N-donor residues (Lys199 and His242).[30] These residues, which can substitute for metal compound ligands that bind to the HSA IIA subdomain, can converge to the metal center.[33,34] Therefore, to enhance the delivery efficiency, selectivity, and anticancer activity of the Fe agent, Fe anti-cancer pro-drug with two leaving groups that initially binds to the HSA IIA sub-domain was created. It then binds to Lys199 and His242 of HSA, displacing the Fe pro-drug's leaving groups. Subsequently, Lys199 and His242 of HSA are protonated in the cancer cell's lysosomal acidic environment, which decreases its coordination ability with Fe ion. This allows the Fe agent to be released from the HSA carrier (Figure 1). Furthermore, liver cancer, which has become very common across the globe, is responsible for a large number of cancer deaths.[35] Taking into consideration the above factors, a model was created using Fe agents derived from thiosemicarbazones and liver cancer (Bel-7402) cells to design anticancer Fe pro-drugs based on the N-donor residues (Lys199 and His242) of HSA. The following studies were carried out: (1) design and synthesis of six 2-Hydroxy-1-naphthaldehyde-thiosemicarbazone Fe(III)-Schiff base anticancer compounds (**7**-**12**) (Figure 2), followed by investigation of their structure-activity relationships on Bel-7402 cells; (2) provided feasibility evidence of developing Fe pro-drugs based on N-donor residues of the HSA carrier IIA subdomain; (3) compared *in vivo* targeting ability, therapeutic efficacy, and side effects of the HSA complex to the Fe compound; (4) investigated the release behavior of the Fe

compound from HSA and the possible mechanism for HSA complex penetrating cancer cells; (5) determined the potential anticancer mechanism of the Fe compound/HSA complex.

RESULTS

This study focuses on Fe compounds containing the tridentate 2-Hydroxy-1-naphthaldehyde thiosemicarbazone Schiff-base ligands (TsS) for the following reasons: (1) TsS ligands themselves are promising anticancer agents;[36] (2) hydrophobic properties of the benzyl and alkyl components can facilitate targeting of the hydrophobic binding sites of the HSA IIA subdomain by the Fe compound. Therefore, the TsS ligand was designed to complex with the Fe compounds (pharmacophore), and to then allow for the two Cl atoms to be potential leaving groups (Figure 2).

Design and structure of Fe compounds

It was determined by Richardson et al. that modification at the N4 position of a thiosemicarbazone can effectively increase lipophilicity and produce superior antiproliferative activity.[12] Thus, we performed this modification with alkyl or phenyl groups to investigate the structure-activity relationships of Fe (III) compounds (Figure 2). The following six Fe (III) compounds were synthesized according to the same method. The single crystals of compounds (compound **7-12**), suitable for X-ray diffraction were obtained.

Single-crystal structure analysis showed that all compounds are isomorphous. They all have the same skeleton (1 tridentate Schiff base ligand, 1 Fe(III) center, and two

coordinated Cl atoms), and differ only in the modified group of the Schiff base ligand. As shown in Figure 2, the coordination polyhedron around all of the Fe(III) centers forms a distorted square pyramid (τ = 0.43 for compound **7**, 0.27 for compound **8**, 0.34 for compound **9**, 0.11 for compound **10**, 0.12 for compound **11**, and 0.38 for compound **12**). The metal was displaced from the O1/N1/S1/Cl1 basal plane, and the Cl_2 appears at the apex. The ligand and metal ion complex forms a five and a six-membered closed loop ring, this coordination can enhance the stability of complexes. We examined the antitumor activity (see Biological Studies) and considered the probability of its involvement in the thiosemicarbazone activity to determine the crystal structure of each Fe complex.

Feasibility of developing Fe pro-drug based on the N-donor residues of HSA IIA subdomain

HSA fluorescence (~347 nm) was gradually suppressed with the increase of compound **12** concentrations, at pH 4.7 and 7.4 (Figure S1A and B). This indicates that the Fe compounds bind close to the HSA IIA subdomain. The MALDI-TOF-MS spectrum shows an increase of 366 Da for the HSA complexes, relative to pure HSA. This is equivalent to the molecular weight of *ca.* one compound **12** (Figure S1C). Furthermore, the electrospray ionization mass spectrometry (ESI-MS) of products released from the HSA-**12** complex at pH 4.7, showed an intense signal at *m/z* = 368.04 (Figure S2). This was identified with isotopic envelopes corresponding to [compound **12**]$^{2+}$ (fit: 368.05), implying that two Cl atoms are lost from compound **12**.

We needed to resolve the structure of the HSA-PA-**12** complex in order to gather feasibility evidence for developing Fe pro-drugs based on Lys199 and His242 residues of the HSA IIA subdomain. Electron density maps of the compound **12** compound complexed with HSA reveal the presence of one compound **12** molecule at the IIA subdomain (Figure 3A). The compound **12** bound to the HSA-PA complex is heart-shaped (Figure 3B) and in the HSA IIA subdomain, the Fe compound binds to a large hydrophobic pocket, which is surrounded by residues, including Arg218, Arg222，Lys199, Trp214, Leu219, Phe223, Leu238, His242, Arg257, Leu260, Ile264, Ser287, Ile290, and Ala291 (Figure 3C). Lys199 and His242 replaced two Cl atoms of compound **12**, within the HSA-PA-**12** complex structure and they coordinate with Fe^{3+} (Figures 3A and C). Comparing binding site and binding mode of compound **12** to HSA with *cis*platin and $[RuCl_5(ind)]^{2-}$, we found that they bind to HSA by residue(s) of HSA displacing the ligand(s) in metal compounds, coordinated to metal.[32, 37] Interestingly, *cis*platin can not bind to IIA subdomain, but $[RuCl_5(ind)]^{2-}$ and compound **12** could bind to IIA subdomain. Obviously, the molecular structure and geometry of metal compounds play an important role in their binding site and binding mode in HSA.

Structure-activity relationships of anticancer Fe compounds *in vitro*

Fe compounds have higher cytotoxicity against Bel-7402 cells than the ligands and Fe^{3+} alone (Table 2), implying that the chelation of Fe^{3+} to ligands is the reason that the Fe compounds have such high cytotoxicity. The cytotoxicity of Fe compounds against Bel-7402 cells ($\leq 13.36 \pm 1.35$ μM) is slightly higher than that of cisplatin

(14.54 ± 0.85 μM). Among the six Fe compounds studied, compound **7** has the lowest cytotoxic activity against Bel-7402 cells (13.36 ± 1.35 μM). When, compared to compound **7**, where one H atom attached to the N4 of thiosemicarbazone is replaced by a methyl or aryl group, as in compound **8** and compound **9**, the cytotoxic activity is enhanced (11.87 or 2.22 μM). The Fe compounds derived from thiosemicarbazone where both of the H atoms at the N4 position are altered, i.e., in (compound **10**, compound **11**, and compound **12**), even higher cytotoxicity is observed (0.86−0.65 μM) (Table 2). The Fe compounds in complexation with HSA increase their cytotoxicity in Bel-7402 cells by approximately 2–6 fold, relative to the Fe compounds alone; however, in normal cells [immortalized human hepatocyte cells (HL7702)], they do not raise cytotoxicity levels (Table 2). As compound **12** and HSA-**12** complex have high cytotoxic activity on Bel-7402 cells, relative to other Fe compounds *in vitro*, these were selected for further investigation.

***In vivo* animal studies of compound 12 and HSA-12 complex**

To further evaluate combining the HSA carrier with pro-drug strategies for the therapeutic efficacy of Fe compound *in vivo*, the liver cancer Bel-7402 xenograft mouse model was established.

Acute toxicity of compound 12 and HSA-12 complex *in vivo*

We measured levels of creatine kinase (CK), blood urea nitrogen (BUN), aspartate aminotransferase (AST), and alkaline phosphatase (ALT) 3 days after intravenous injection of the drugs in order to assess acute toxicity of compound **12** and HSA-**12** complex in the heart, kidney, and liver of normal mice. Levels of CK in compound

12-treated mice were greater than levels in the control (NaCl) group. However, the levels of CK in the HSA-**12** complex-treated mice were similar to those of the control. This indicates that HSA-**12** complex has low cardiotoxicity. High BUN levels correspond to higher toxicity in the kidney. compound **12** caused significant nephrotoxicity, as evidenced by a higher level of BUN than that observed in the control group. In contrast, BUN levels significantly decreased in the HSA-**12** complex-treated groups, indicating lower nephrotoxicity. Serum AST and ALT levels were significantly elevated in the group treated with compound **12**; however, the levels induced by HSA-**12** complex were almost the same as the control group, which indicates lower levels of liver damage in those treated with HSA-**12** complex.

Anti-tumor activity of compound 12 and HSA-12 complex *in vivo*

Bel-7402 tumor-bearing mice were injected with compound **12** and HSA-**12** complex and saline was injected as a control to evaluate therapeutic efficacy. Tumor-bearing mice had their body weight and tumor volume monitored every 2 days for 28 days. At the end of the experiment, the tumor volumes in the HSA-**12** complex-treated mice were much smaller than those in saline-treated and compound **12**-treated mice (Figure 4A). Compared to the control group, the tumor volume after 28 days treatment was 53.2 ± 4.5% for the compound **12** group and 24.6 ± 2.8% for the HSA-**12** complex group, demonstrating that HSA-**12** complex resulted in greater tumor growth inhibitory efficacy than compound **12**. Compared to the NaCl group, the tumor inhibition rate (TIR) of HSA-**12** complex was 75.6% ($P < 0.001$), which was significantly higher than that of compound **12** (46.8%, $P < 0.01$).

To further evaluate the antitumor effects of compound **12** and HSA-**12** complex in animals, the tumor tissues were excised for pathology. The TUNEL stained tissue sections indicate obvious differences in tumor tissue morphology between treated groups and the NaCl group (Figure 4B). As shown in Figure 4B, tumor samples from animals treated with compound **12** and HSA-**12** complex showed increased apoptosis compared with tumor samples from the control mice. In particular, HSA-**12** complex was more effective in promoting cell necrosis, relative to compound **12**.

Comparison of the side effects of compound 12 and HSA-12 complex *in vivo*

To evaluate the toxicology of compound **12** and HSA-**12** complex in mice, mouse body weight was monitored throughout the intravenous treatment. At the end of the study, specific organs were collected and weighed (Table S3). When compared with the control mice, those intravenously treated with HSA-**12** complex, did not show significant weight loss ($p > 0.05$). In contrast, mice treated with compound **12** lost approximately 10% of their body weight (Figure 5A). The weight of the liver and heart of mice treated with compound **12** altered slightly, but no change was observed in mice treated with HSA-**12** complex (Table S3) and there was not a significant difference in the weight of the other organs when comparing the HSA-**12** complex-treated and the control groups (Table S3). Pathological sections stained with H&E revealed drug-related side effects to major organs (Figure 5B). Serious damage to the heart (vacuolation), liver (vacuolation), and kidneys (focal abnormalities) was observed in mice treated with compound **12**. This damage was significantly decreased in mice treated with the HSA-**12** complex. Therefore, increased liver and heart

weights are likely attributed to increased vacuolation.

Selectivity of HSA complex *in vivo*

To evaluate whether the HSA complex selectively accumulates in the Bel-7402 tumor *in vivo*, the Fe content in tumors of mice treated with compound **12** and HSA-**12** complex, was measured. Using inductively coupled plasma atomic emission spectrometry (ICP-AES), the iron content in tumors treated with HSA-**12** complex is significantly ($p<0.05$) higher compared to those treated with compound **12**. This data suggests that the HSA complex selectively accumulates in tumors. Furthermore, the data also indicates that the HSA complex decreased Fe compound accumulation in the liver and kidney (Figure 6A).

Fe pro-drug release from HSA

To examine the release behavior of Fe from HSA in different environments, the environment inside the cancer cell was stimulated, and the compound **12** released from the HSA carrier was measured in buffers of pH 4.7 and pH 7.4. Approximately 5% of the Fe compound was released from the HSA complex within 48 h in pH 7.4 buffer, whereas up to 80% of Fe compound was released from HSA in pH 4.7 buffer (Figure 6B). In addition, the binding affinity of Fe compound to HSA in pH 7.4 buffer [K = 6.88 (±0.08) × 10^6 M^{-1}] was significantly greater than that of HSA to Fe compound in pH 4.7 buffer [K = 4.75 (±0.05) × 10^4 M^{-1}]. These results indicate that Fe compound bind weakly to, and are more easily released from, HSA in an acidic environment.

Possible mechanism of HSA-12 complex absorbed by cancer cells

It was determined by Desai et al. that after interacting with SPARC (Secreted Protein, Acid, and Rich in Cysteine) on tumor cell surfaces, HSA penetrates the cell membrane by the process of caveolae protein mediated endocytosis.[38,39] To determine if a similar mechanism for HSA-**12** complex penetration into Bel-7402 cells is observed here, the organization of caveolae was disturbed by treating Bel-7402 cells with methyl-β-cyclodextrin, a known endocytosis inhibitor.[40] The HSA and Fe permeability were then measured. Compared with the control (0 mM of methyl-β-cyclodextrin), the amount of intracellular HSA and Fe in cells incubated with methyl-β-cyclodextrin was reduced (Figure 7). In addition, the amount of intracellular HSA and Fe in cells incubated with l mM methyl-β-cyclodextrin is more than that of cells incubated with 2 mM methyl-β-cyclodextrin (Figure 7). These results affirm that the Fe cell content is explicitly proportional to the HSA cell content. This indicates that methyl-β-cyclodextrin prevents the albumin-induced increase in transendothelial HSA and Fe permeability, which results in reduction of the amount of HSA and Fe in cells. In turn, this suggests that the HSA-**12** complex possible penetrates Bel-7402 cells by endocytosis.

Potential anticancer mechanism of compound 12/HSA-12 complex

DNA transcription and replication require separation of the super-coiled DNA double-helix. Topo-Iiα is responsible for unlinking DNA during replication, which then allows DNA relaxation during transcription and supports chromatin remodeling.[41] Disruption of Topo-IIα leads to double-strand DNA breaks, ultimately causing cell death. This has led to the identification of Topo-IIα as one of the most

important clinical targets for modern cancer chemotherapy, and its inhibitors are the central components of many therapeutic regimens.[42] Recently, many reports have acknowledged that thiosemicarbazone derivatives likely target Topo-IIα[42-45] so we decided to evaluate the use of human Topo-IIα-mediated pBR322 relaxation and kDNA decatenation assays to determine if the compound **12** compound can indeed inhibit Topo-Iiα. The results show that the compound **12** significantly inhibits Topo-IIα activity, suggesting compound **12** is a potent Topo-IIα inhibitor (Figure 8A).

Topo-IIα inhibition is thought to affect cell cycle.[41] Thus, we investigated the influence of compound **12** and HSA-**12** complex on the cell cycle distribution in human liver cancer cells using flow cytometric DNA content analysis. We noted that in the S phase, when treated with compound **12**, the percentage of cells increased from 27.78% to 42.10% than when treated with HSA-**12** complex. The control cells, with no drug treatment, had 19.99% of cells in the same phase (Figure 8B). The Fe(III) compound and HSA complex may cause cell accumulation in the S phase of the cell cycle by either delaying or inhibiting progression to the next phase. Cell cycle regulatory protein expression, including that of cyclins and cyclin-dependent kinases, was investigated to elucidate the molecular mechanism underlying the S phase arrest induced by Fe(III) compound and HSA complex in Bel-7402 cells. compound **12** increased the expression of cyclins E and A (Figure 8D), which associate with Cdk2; the resulting complexes, cyclin E/Cdk2 and cyclin A/Cdk2, regulate the initiation and progression of the S phase, respectively.[46,47] The expression of cyclin E and cyclin A was high after 24 h, which suggests that compound **12** persevered in enhanced S

phase progression and compound **12** caused increased E2F-1 expression (which promotes cyclin E and A transcription) at 24 h (Figure 8D).[48] The enhanced expression of cyclin E and A and E2F-1 appear to be directly responsible for the compound **12**-induced S phase arrest.

Many studies have affirmed that metal compounds can introduce reactive oxygen species (ROS) into cancer cells.[49] Increased ROS can damage macromolecules and alter cell function or induce apoptosis.[50] To investigate if compound **12** and HSA-**12** complex can produce ROS in Bel-7402 cells, a fluorescent DCF probe and flow cytometry were utilized. The cells treated with compound **6** and compound **12** or HSA-**12** complex have greater DCF fluorescence intensity and a right shifted peak relative to control cells (Figure 9A). compound **6** does not obviously increase ROS compared to control cells after 24 h. However, compound **12** significantly ($p < 0.001$) increased H_2DCF oxidation 223 ± 20% after 24 h incubation. Thus, compound **12** produces significantly ($p < 0.001$) more ROS than compound **6** (105 ± 20%), but did not produce as much as HSA-**12** complex (355 ± 20%). Prior studies have confirmed that Fe compounds introduce reactive oxygen species *via* redox-cycling. In their reduced (Fe^{II}) form, these complexes can react with molecular oxygen; the resulting ferric complexes may subsequently interact with cellular reductants. Voltammograms were recorded to determine if compound compound **12** can generate reactive oxygen species through the reduction of Fe^{III} to Fe^{II} (Figure 9B). Redox potentials of the compound **12** compound are relatively high, suggesting that the Fe^{III} compound can be easily reduced and then able to take part in redox cycling and ROS generation.

Increased ROS and mitochondrial dysfunction are related apoptosis events.[50,51] The apoptosis process is mediated by the mitochondrial/apoptotic cascade and is often linked with mitochondrial membrane changes caused by the leakage of pro-apoptotic factors.[52] The lipophilic fluorescent probe JC-1 (5, 5, 6, 6′-tetrachloro-1, 1′, 3, 3′-tetraethyl-imidacarbocyanine iodide) was used to measure mitochondrial membrane potential changes (Δψm). JC-1 staining indicates decreased Δψm, as evidenced by less red fluorescence (JC-1 aggregates) and increased green fluorescence (JC-1 monomers).[49] Bel-7402 cells were then treated with 1 μM of $FeCl_3$, compound **6**, compound **12**, or HSA-**12** complex for 24 h and Δψm was decreased (Figure 9C). Mitochondrial-mediated apoptosis activation was confirmed and each compound's ability to decrease Δψm was consistent with *in vitro* cytotoxicity. BeL-7402 was incubated with $FeCl_3$ and compound **6** for 24 h, which decreased Δψm (3.46% and 5.52%, respectively) ($p < 0.05$), and a significant ($p < 0.001$) decrease in Δψm was observed after incubation with compound **12** (12.0%) or HSA-**12** complex (22.2%) (Figure 9C).

Topo-IIα inhibition could potentially lead to an attack on components of DNA, DNA strand breaks, DNA intra-strand adducts, and DNA–protein crosslinks.[41] Transcription factor p53 is another major player in apoptosis or cell cycle arrest response of cells to DNA damage. Western blotting was used to detect changes of p53 to determine if compound **12** and HSA-**12** complex had caused DNA damage. Pretreatment with HSA-**12** complex enhanced radiation-induced DNA damage more than compound **12**, as evidenced by increased p53 phosphorylation levels as shown in

Figure 10. The Bcl-2 protein family are thought to be key regulators of Δψm.[53,54] Thus, Western blotting was used to determine if compound **12** or HSA-**12** complex significantly ($p < 0.001$) upregulated Bax expression (pro-apoptotic Bcl-2 protein family) and suppressed expression of Bcl-2 and Bcl-xl (pro-survival Bcl-2 family proteins). We determined that the ratio of Bcl-2/Bax was decreased, which indicates that Bcl-2 proteins regulated the loss of Δψm. HSA-**12** complex significantly upregulated the expression of Bax and suppressed Bcl-2 and Bcl-xl expression in BEL-7402 cells in comparison to compound **12** ($p < 0.001$). In addition, Western blotting revealed that cytochrome c (Cyt C) and the caspase protein family (caspase-3 and -9) were greatly upregulated ($p < 0.001$), suggesting that Cyt C was the cause of caspase-3 and -9 activation. Results show that HSA-**12** complex is significantly ($p < 0.001$) more effective in up-regulating caspase family protein expression and Cyt C in Bel-7402 cells, compared to compound **12**.

We used Annexin V-FITC/PI staining to further valid compound **12** and HSA-**12** complex's ability to bolster cell apoptosis; the data showed Bel-7402 cell apoptosis of 10.3% for compound **12** and 20.9% for HSA-**12** complex (Figure 10C). Results show that HSA-**12** complex is significantly ($p < 0.001$) more effective at promoting Bel-7402 cell apoptosis compared to compound **12**.

DISCUSSION

The study demonstrated that the anticancer activity of ligands may be enhanced by coordinating with complexes containing Fe(III). The nature of the Fe-bound ligand directly affected the anti-cancer properties of the Fe compound and lipophilic groups

attached to the ligand also played an important role in increasing the anti-cancer activity of the potential Fe therapeutic. When we replaced the H atom in the N4 location of the ligand with a more lipophilic functional moiety, such as an alkyl or aryl group, the other five Fe(III) compounds we investigated showed a one- to twenty-fold increase in anti-cancer activity relative to compound **7** (Table 1), and the Fe(III) compound is proportional to the degree of lipophilicity of the ligand. With the basic pharmacophore of the ligand attached to Fe(III) left intact, lipophilic groups of the ligand could be modified in an attempt to regulate the anti-cancer activity of the Fe(III) compound.

There is the potential to increase anticancer activity and metal drug selectivity by altering the carrier; however, efficacy of *in vivo* drug delivery and the ability to release in cancer cells need to be simultaneously taken into consideration. Yang et al. has proposed a new strategy for designing metal pro-drug that is based on the nature of the cancer cells and the HSA IIA subdomain.[32-34] The results of this study confirm that it is feasible to design an Fe pro-drug according to Yang et al.'s proposal. By examining the HSA complex structure, it was determined that Lys199 and His242 replaced two Cl atoms of the Fe compound, and coordinated with Fe(III), which enables the Fe compound to forge a strong bond in the hydrophobic cavity of the HSA IIA subdomain. As a result, minimal Fe compound (about 5%) is released from HSA at pH 7.4, whereas approximately 80% of Fe compound are released from HSA in acidic environments (pH 4.7). This is due to a dramatic decrease in the Fe compound binding affinity in these two environments. Based on these release profiles, it is

suggested that the HSA complex will be stable in blood during *in vivo* circulation, and that the Fe compound will be released after there is a selective accumulation of acid lysosome in the cancer cells.

The therapeutic efficiency of compound **12**/HSA-**12** complex *in vivo* was evaluated by considering three factors: TIR, side effects, and selectivity, in mice. The TIR of the FA-HSA-**12** complex treated mice almost reached 75.6%, and was 1.6 times higher than that of the compound **12** treated group. FA-HSA-**12** complex is well tolerated in mice and causes less weight loss relative to compound **12** alone. H&E staining indicated that HSA-**12** complex can effectively reduce the heart, liver, and kidney damage induced by free compound **12**. Furthermore, the ICP-AES results show that HSA-**12** complex facilitates Fe compound accumulation in the tumor *in vivo*. The liver cancer xenograft experiments in mice further indicate that HSA complexation is helpful for decreasing side effects, improving anti-tumor activity and selectivity of Fe compound. Furthermore, the HSA complex has a lower toxicity against normal cells and tissues than the Fe compound. This is due to a more selective accumulation of the HSA complex in tumor cells, enhanced permeability, and the retention (EPR) effect of the macromolecule in tumors (Figure 11).[37-39]

These results confirm that the HSA complex has a better therapeutic efficacy and lower systemic toxicity, than free compound **12**. The principle of the classic approach for developing metal anticancer drugs is for their them to quickly replicate and speed up the mitotic processes of malignant cells.[5] However, there are still some major drawbacks concerning these metal drugs: they only work with certain types of cancers;

some tumors may have acquired or intrinsic resistance; and they often have severe side effects.[7] Therefore, new approaches are needed to develop cancer drugs that circumvent these drawbacks. Among these, developing anticancer drugs that target proteins related to cancer may be promising. Excitingly, the results outlined here show that Fe compounds eradicate cancer cells using multiple anticancer mechanisms, such as regulating the expression of proteins in cancer cells. Furthermore, the anticancer capacity of the Fe compound is improved when complexed with HSA, relative to the Fe compound alone. Therefore, it is necessary to create a multi-target anticancer Fe pro-drug based on the HSA carrier that improves delivery efficiency and increases anticancer activity and selectivity while overcoming resistance.

CONCLUSION

Due to His242 and Lys199 replacing the groups of Fe pro-drug that have left and then coordinating with Fe^{3+}, certain aspects of Fe compounds have improved, including delivery efficiency, anticancer activity, and selectivity, since they bind strongly to the IIA subdomain of HSA. Compared to the Fe compound alone, the HSA complex showed better tolerance, higher drug accumulation in tumor tissues, and lower toxicity, indicating that it had superior anti-tumor activity and was associated with milder side effects. These results suggest that the HSA carrier pro-drug strategy for intravenous administration of novel, active thiosemicarbazone containing Fe(III) compounds, may be a promising approach for targeted cancer therapy.

Experimental Section

Chemicals and reagents. HSA (fatty acid content <0.05%) was purchased from

Sigma-Aldrich (Shanghai, China) and used without requiring further purification. All other chemicals and solvents were of high purity and are available from commercial sources. Distilled water was used in the reactions. Elemental analyses (C, N, H, and S) were carried out on a Perkin-Elmer 2400 analyzer. We use the x-ray diffraction to determine the compounds structure, and element analysis (C, H, N, S) to determine the purity of compounds are ≥ 95%.

Synthesis and characterization of ligands. The ligands compound **1-6** were prepared according to the following procedures.[4,36] In brief; the thiosemicarabazide (10 mmol) and 2-Hydroxy-1-naphthaldehyde (10 mmol) were combined in methanol (20 mL) with acetic acid (1-2 drops). While the mixture was boiled, a white or off-white precipitate appeared; after 4 h, it was allowed to cool at room temperature. The mixture was subsequently filtered, washed with cold water, and dried *in vacuo*.

2-Hydroxy-1-naphthaldehyde-thiosemicarbazide (1). Yield: 8.24 mmol (82.4%). Anal. Calcd (%) for $C_{12}H_{10}N_3OS$: C, 59.00; H, 4.13; N, 17.20; O, 6.55; S, 13.13. Found: C, 59.05; H, 4.10; N, 17.21; O, 6.51; S, 13.13. IR, cm^{-1}: 3698 (m, OH), 3449 (s, amide), 3256 (s, NH), 3165 (m, aromatic hydrogen), 1607 (s), 1573 (s), 1510 (s), 1471 (s, aromatic), 1394 (s, C=N), 1328 (s, thioamide), 1238 (s), 1118 (s), 880 (m), 819 (m, C-H), 748 (m, C=S), 647 (m). ESI^+ m/z: calcd for $C_{12}H_{10}N_3OS$, 244.02 [M - H].

2-Hydroxy-1-naphthaldehyde-4-methylthiosemicarbazide (2). Yield: 7.96 mmol (79.6%). Anal. Calcd (%) for $C_{13}H_{13}N_3OS$: C, 60.44; H, 4.68; N, 16.27; O, 6.19; S, 12.41. Found: C, 60.40; H, 4.65; N, 16.30; O, 6.16; S, 12.48. IR, cm^{-1}: 3702 (m, OH),

3419 (s, amide), 3201 (s, NH), 3007 (m, aromatic hydrogen), 1620 (m), 1596 (s), 1532 (s), 1428 (s, aromatic), 1397 (m, C=N), 1330 (s, thioamide), 947 (s), 888 (s, C-H), 776 (m), 744 (m), 716 (m, C=S), 684 (m). ESI^+ m/z: calcd for $C_{13}H_{13}N_3OS$, 258.06 [M - H].

2-Hydroxy-1-naphthaldehyde-4-phenylthiosemicarbazide (3). Yield: 85.5 mmol (85.5%). Anal. Calcd (%) for $C_{18}H_{15}N_3OS$: C, 67.27; H, 4.70; N, 13.07; O, 4.98; S, 9.98. Found: C, 67.22; H, 4.73; N, 13.03; O, 4.99; S, 10.13. IR, cm^{-1}: 3711 (m, OH), 3385 (s, amide), 3151 (s, NH), 3000 (m, aromatic hydrogen), 1621 (m), 1595 (s), 1542 (s), 1442 (m, aromatic), 1415 (m, C=N), 1326 (s, thioamide), 1094 (s), 939 (s, C-H), 902 (m), 856 (m), 766 (m, C=S), 719 (m). ESI^+ m/z: calcd for $C_{18}H_{15}N_3OS$, 320.10 [M - H].

2-Hydroxy-1-naphthaldehyde-4,4-dimethylthiosemicarbazide (4). Yield: 9.01 mmol (90.1%). Anal. Calcd (%) for $C_{14}H_{15}N_3OS$: C, 61.51; H, 5.53; N, 15.37; O, 5.85; S, 11.73. Found: C, 61.51; H, 5.53; N, 15.37; O, 5.85; S, 11.73. IR, cm^{-1}: 3739 (m, OH), 3279 (s, amide), 3039 (s, NH), 3000 (m, aromatic hydrogen), 1619 (s), 1548 (m), 1520 (s), 1462 (s, aromatic), 1357 (m, C=N), 1238 (s, thioamide), 1181 (s), 1141 (s), 906 (m), 884 (m, C-H), 650 (m, C=S), 594 (m). ESI^+ m/z: calcd for $C_{14}H_{15}N_3OS$, 272.09 [M - H].

2-Hydroxy-1-naphthaldehyde-4,4-diethylthiosemicarbazide (5). Yield: 7.90 mmol (79.0%). Anal. Calcd (%) for $C_{16}H_{19}N_3OS$: C, 63.76; H, 6.35; N, 13.94; O, 5.31; S, 10.64. Found: C, 63.74; H, 6.36; N, 13.90; O, 5.33; S, 10.67. IR, cm^{-1}: 3715 (m, OH), 3293 (s, amide), 2982 (s, NH), 2934 (m, aromatic hydrogen), 1620 (m), 1590 (m),

1538 (s), 1462 (s, aromatic), 1414 (s, C=N), 1356 (s, thioamide), 1271 (m), 1133 (s), 1074 (m), 955 (m, C-H), 803 (m, C=S), 694 (m). ESI^+ m/z: calcd for $C_{16}H_{19}N_3OS$, 300.13 [M - H].

2-Hydroxy-1-naphthaldehyde-3-piperidinethiosemicarbazide (6). Yield: 7.43 mmol (74.3%). Anal. Calcd (%) for $C_{17}H_{19}N_3OS$: C, 65.15; H, 6.11; N, 13.41; O, 5.10; S, 10.23. Found: C, 65.10; H, 6.13; N, 13.42; O, 5.9; S, 10.26. IR, cm^{-1}: 3640 (m, OH), 3323 (s, amide), 3204 (s, NH), 2964 (m, aromatic hydrogen), 1620 (s), 1594 (s), 1537 (s), 1465 (s, aromatic), 1403 (s, C=N), 1326 (s, thioamide), 1252 (s), 1180 (s), 1084 (m), 957 (m, C-H), 822 (m, C=S), 746 (m). ESI^+ m/z: calcd for $C_{17}H_{19}N_3OS$, 312.13 [M - H].

Synthesis and characterization of Fe compounds. The compounds compound **7-12** were synthesized as the following methods. The relevant ligands (1 mmol) were dissolved in MeOH (10 mL) over gentle heat and stirred. A solution of $FeCl_3$ (0.20 g, 1 mmol) in MeOH (10 mL) was added dropwise and stirred, and the ligand solution immediately turned dark brown. Fine dark brown crystals formed upon standing, which were then filtered off, washed with EtOH (5 mL) and diethyl ether (5 mL) was added.

2-Hydroxy-1-naphthaldehyde-thiosemicarbazide-iron(III)-bischlorin (7). Yield: 0.65 mmol (65%). CCDC NO. 1442009. Anal. Calcd (%) for $C_{12}H_9Cl_2FeN_3OS$: C, 38.95; H, 2.45; N, 11.36; O, 4.32; S, 8.67. Found: C, 38.98; H, 2.40; N, 11.32; O, 4.36; S, 8.69. IR, cm^{-1}: 3246 (s, amide), 3038 (s, NH), 2961 (m, aromatic hydrogen), 1615 (s), 1595 (s), 1573 (s), 1457 (s, aromatic), 1388 (s, C=N), 1337 (s, thioamide), 1196

(s), 1165 (s), 1146 (m), 974 (m, C-H), 821 (m, C=S), 749 (s). ESI$^+$ m/z: calcd for $C_{12}H_9Cl_2FeN_3OS$, 369.03 [M - H].

2-Hydroxy-1-naphthaldehyde-4-methylthiosemicarbazide-iron(III)-bischlorin (8). Yield: 0.57 mmol (57%). CCDC NO. 1442010. Anal. Calcd (%) for $C_{13}H_{11}Cl_2FeN_3OS$: C, 40.65; H, 2.89; N, 10.94; O, 4.17; S, 8.35. Found: C, 40.59; H, 2.85; N, 10.96; O, 4.19; S, 8.41. IR, cm^{-1}: 3288 (s, amide), 3005 (s, NH), 2974 (m, aromatic hydrogen), 1608 (s), 1534 (s), 1477 (s), 1447 (s, aromatic), 1359 (s, C=N), 1337 (s, thioamide), 1194 (s), 1142 (m), 970 (m, C-H), 823 (m, C=S), 756 (s), 603 (s), 561 (s). ESI$^+$ m/z: calcd for $C_{13}H_{11}Cl_2FeN_3OS$, 383.06 [M - H].

2-Hydroxy-1-naphthaldehyde-4-phenylthiosemicarbazide-iron(III)-bischlorin (9). Yield: 0.54 mmol (54%). CCDC NO. 1442011. Anal. Calcd (%) for $C_{18}H_{13}Cl_2FeN_3OS$: C, 48.46; H, 2.94; N, 9.42; O, 3.59; S, 7.19. Found: C, 48.43; H, 2.95; N, 9.40; O, 3.58; S, 7.24. IR, cm^{-1}: 3173 (s, amide), 3014 (s, NH), 2874 (m, aromatic hydrogen), 1595 (s), 1571 (s), 1531 (s), 1456 (m, aromatic), 1389 (s, C=N), 1358 (s, thioamide), 1190 (s), 1139 (s), 1087 (m), 974 (m, C-H), 824 (m, C=S), 747 (s), 699 (s), 651 (m). ESI$^+$ m/z: calcd for $C_{18}H_{13}Cl_2FeN_3OS$, 444.06 [M - H].

2-Hydroxy-1-naphthaldehyde-4,4-dimethylthiosemicarbazide-iron(III)-bischlorin (10). Yield: 0.48 mmol (48%). CCDC NO. 1442012. Anal. Calcd (%) for $C_{14}H_{13}Cl_2FeN_3OS$: C, 42.24; H, 3.29; N, 10.56; O, 4.02; S, 8.05. Found: C, 42.21; H, 3.26; N, 10.59; O, 4.04; S, 8.06. IR, cm^{-1}: 3248 (s, amide), 2986 (s), 2934 (m, aromatic hydrogen), 1592 (s), 1536 (s), 1507 (s), 1454 (s, aromatic), 1393 (s, C=N), 1362 (s, thioamide), 1241 (s), 1197 (s), 1165 (m), 976 (m, C-H), 830 (m, C=S), 749

(s). ESI$^+$ m/z: calcd for $C_{14}H_{13}Cl_2FeN_3OS$, 396.06 [M - H].

2-Hydroxy-1-naphthaldehyde-4,4-diethylthiosemicarbazide-iron(III)-bischlorin (11). Yield: 0.39 mmol (39%). CCDC NO. 1442013. Anal. Calcd (%) for $C_{16}H_{17}Cl_2FeN_3OS$: C, 45.10; H, 4.02; N, 9.86; O, 3.75; S, 7.52. Found: C, 45.13; H, 4.04; N, 9.80; O, 3.71; S, 7.57. IR, cm^{-1}: 3256 (s, amide), 3055 (s), 2974 (m, aromatic hydrogen), 1570 (s), 1507 (s), 1434 (s, aromatic), 1389 (s, C=N), 1353 (s, thioamide), 1197 (s), 1143 (s), 1086 (m), 975 (m, C-H), 827 (m, C=S), 746 (s). ESI$^+$ m/z: calcd for $C_{16}H_{17}Cl_2FeN_3OS$, 424.09 [M - H].

2-Hydroxy-1-naphthaldehyde-3-piperidinethiosemicarbazide-iron(III)-bischlorin (12). Yield: 0.55 mmol (55%). CCDC NO. 1442014. Anal. Calcd (%) for $C_{17}H_{17}Cl_2FeN_3OS$: C, 46.60; H, 3.91; N, 9.59; O, 3.65; S, 7.32. Found: C, 46.56; H, 3.93; N, 9.57; O, 3.68; S, 7.33. IR, cm^{-1}: 2924 (s, amide), 2807 (s), 2758 (m, aromatic hydrogen), 1595 (s), 1576 (s), 1536 (s), 1464 (s, aromatic), 1356 (s, C=N), 1319 (s, thioamide), 1243 (s), 1185 (s), 969 (m, C-H), 826 (m, C=S), 749 (s). ESI$^+$ m/z: calcd for $C_{17}H_{17}Cl_2FeN_3OS$, 437.14 [M - H].

Crystal structures determination of Fe compounds. X-ray crystallographic data were collected on a Bruker SMART Apex II CCD diffractometer using graphite-monochromated Mo-Kα (λ = 0.71073 Å) radiation. Empirical adsorption corrections were applied to all data using SADABS. Direct methods were used to solve the structures and they were then refined against F^2 by full-matrix least-squares methods using SHELXTL (version 5.1).[55] All of the non-hydrogen atoms were refined anisotropically while all of the other hydrogen atoms were placed in ideal geometric

positions and constrained to ride on their parent atoms. The crystallographic data for compound **7-12** are summarized in Table S1 and selected bond lengths and angles are given in Table S2. Crystallographic data for the structural analyses were deposited at the Cambridge Crystallographic Data Centre and assigned reference numbers 1442009-1442014. The crystallographic data can be obtained free of charge from the Cambridge Crystallographic Data Centre *via* http://www.ccdc.cam.ac.uk/data_request/cif.

X-ray crystallography of HSA complex. Fatty acid (FA) free HSA was purified by removing HSA dimers and multimers as published.[56] Palmitic acid (PA) was dissolved in alcohol and diluted to 2.5 mM with 20 mM potassium phosphate (pH 7.5). HSA complexes were prepared by mixing 100 μL HSA (100 mg/mL), 380 μL PA (2.5 mM), and 90 μL of each Fe compound (5 mM) overnight. Mixtures were then concentrated to 100 mg/ml with a Millipore spin filter (10,000 Dalton Cut-off). Crystallization was induced using the sitting drop vapor diffusion method at room temperature. An equal volume of the HSA complex was mixed with the reservoir solution, which contained 28–32% (w/v) polyethylene glycol 3350, 50 mM potassium phosphate (pH 7.5), 5% glycerol, and 4% DMSO. Crystals were directly selected from the drop solution and then frozen in liquid nitrogen.

X-ray diffraction data were collected under Cryo-conditions (100 K) at BL17U beamline of Shanghai Synchrotron Radiation Facility and then integrated and scaled with HKL2000.[57] The HSA complex structure were solved by molecular replacement using PHASER in PHENIX suites with initial model of HSA-MYR structure

(PDB:1BJ5) but stripped the ligand as initial searching model, all ligands were built into the model by LigandFit in PHENIX and manually modified and adjusted in COOT.[56,58,59] The HSA structure was refined in PHENIX at resolution of 2.80 Å, with R_{factor}=0.209 and R_{free}=0.267. All residues located in favored or allowed region and no residues located in outlier region by Ramachandran plot in HSA structure, the statistics of data collection and refinement see Table 3. Structure superimposition were done by Chimera (http://www.cgl.ucsf.edu/chimera) and all crystallographic figure were drawn by Pymol (http://www.pymol.org).[60]

In *vitro* anticancer activity

Cell culture. Culture medium DMEM (with L-glutamin), fetal bovine serum (FBS), phosphate buffered saline (PBS, pH = 7.2), and Antibiotice-Antimycotic came from E.U. Gibco BRL. Human hepatocellular cell line Bel-7402 and normal liver cells HL-7702 were purchased from the American Type Culture Collection and the German Collection of Microorganisms and Cell Cultures and maintained in DMEM supplemented with 10% FBS, 50 U/mL of penicillin, and 50 mg/mL of streptomycin at 37 ℃ and 5% CO_2.

Cytotoxicity assay (MTT). One hundred microliters of cell suspension at a density of 5×10^4 cells/mL was seeded in 96-well plates and incubated for 24 h at 37℃ in 5% CO_2. Complexes at various concentrations were then added to the test well. The resultant cell mixture was incubated at 37℃ in a 5% CO_2 atmosphere for 48 h. An enzyme labeling instrument was used to read absorbance with 570/630 nm double wavelength measurement. Cytotoxicity was determined based on the percentage of

cell survival compared with the negative control. The final IC_{50} values were calculated by the Bliss method (n = 5). All of the tests were repeated in triplicate.

***In vivo* animal studies**

Animal subject and tumor models. Athymic nude mice were obtained from Beijing HFK Bioscience Co., Ltd. and used in the study at 6 weeks of age. All animal experiments were carried out in compliance with the Animal Management Rules of the People's Republic of China's Ministry of Health (document NO. 55, 2001) and under the guidelines of the University of Jinan Ethics Committee's Care and Use of Animals. Athymic nude mice were obtained from Beijing HFK Bioscience Co., Ltd. and used in the study at 6 weeks of age. We dissolved the complexes in DMSO solution as mother liquid mixture (10 mM), and then diluted by NaCl solution to the required concentration in vivo experiments.

Acute toxicity study. The acute toxicity of compound **12** and HSA-**12** complex were assessed on normal mice using the method previously described.[61] Briefly, 32 healthy Kunming mice (aged 3～4 weeks and weighing 18～22 g with an equal number of female and male subjects) were divided into four groups, with 8 mice in each group. compound **12** and HSA-**12** complex were administrated into the different groups of mice at doses of 25 μmol Fe/kg body weight. NaCl was injected into the control group. Blood samples from each group of mice were drawn 3 days after intravenous (IV) injection to prepare the serum samples. The serum biochemical parameters of the blood samples were determined: aspartate aminotransferase (AST), alanine aminotransferase (ALT), creatinine kinase (CK), and blood urea nitrogen (BUN).

Finally, the major organs heart, liver and kidney were sectioned for histopathological analysis using hematoxylin and eosin (H&E) staining.

***In vivo* anti-tumor activity study.** The nude mice were subcutaneously injected in the right flank with 200 μL of cell suspension containing 4×10^6 Bel-7402 cells. When the tumor volume was approximately 100 mm^3 for the study, the Bel-7402 tumor-bearing mice were randomly divided into three groups, and mice in different treatment groups were intravenously injected with NaCl, compound **12**, and HSA-**12** complex at doses of 2.5 μmol Fe/kg body weight every 2 days. Each mouse of different group was earmarked and followed individually throughout the whole experiments. The width and length of the tumor and the body weight of mice were measured before every injection by the end of experiment. Volume was determined using the following equation: tumor volume (V) = $1/2 \times$ length $\times$ $width^2$. Mice were killed after 28 days of treatment and tumor tissues and major organs were excised for histopathological analysis with H&E staining.

Hematoxylin and eosin (H&E) staining. Tumor samples were given a routine histopathological examination using standard H&E staining. Small pieces were collected in 4% paraformaldehyde for proper fixation and they were then processed and embedded in paraffin wax. Sections were cut and stained with hematoxylin and eosin and samples were then observed under light microscope using an Eclipse E800 Nikon (Nikon, Tokyo, Japan). Representative images were shown. Quantitative analysis of eosin stained areas in treated tumors expressed as relative amount compared to eosin necrotic area of untreated tumors (± SD), were assessed by area

counting of three fields for each of five slides per each sample at ×10 magnification by Image–ProPlus software (Immaginie Computer, Milan, Italy).

Tunel Assay. The apoptotic cell death was assayed using *in situ* detection of DNA fragmentation with the terminal deoxynucleotidyl-transferase (TUNEL) assay. Paraffin liver cancer tissue sections (5 μm) were warmed for 30 min. (64℃), deparaffinized, and rehydrated. Terminal transferase mediated dUTP nick end-labeling of nuclei was performed using the APO-BrdU TUNEL Assay kit (A-23210; Molecular Probes, Eugene, OR) following the manufacturer's protocol. Samples were then observed under fluorescence microscopy using an Eclipse E800 Nikon (Nikon, Tokyo, Japan). Representative images were shown. Quantitative analysis of TUNEL positive areas expressed as relative amount of treated area compared to untreated ones, were assessed by area counting of three fields for each of five slides per each sample at ×60 magnification by Image–ProPlus software (Immagini e Computer, Milan, Italy).

***In vivo* targeting ability study.** At the end of the *in vivo* experiment, the mice tumors were homogenized and then 0.5 g of the sample was placed in Teflon containers and mineralized in 1 mL of 30% hydrogen peroxide and in 7 mL of concentrated HNO_3 in a microwave apparatus (Milestone MSL 1200) under pressure. The presence of Fe in the mice tumors was determined using inductively coupled plasma atomic emission spectrometry (ICP-AES).

Fe pro-drug release from HSA. The Fe(III) compound release from HSA complex was studied by dialyzing HSA complex at pH 4.7 and 7.5 buffers to simulate cell

matrix and interstitial space environment, respectively. Briefly, 2 mL HSA complex in dialysis pocket were dispersed in tube containing 20 mL pH 4.7 and 7.5 buffers, respectively. To investigate release behavior at different time interval, we prepared for 7 tubes for each pH value. The amount of Fe(III) compound released from the HSA complex was determined by graphite furnace atomic absorption spectrometer (AAS).

Determining the possible mechanism of HSA-12 complex absorbed by cells.

Bel-7402 cells were cultured in 70-mm culture dishes, grown to 70% confluence, and incubated with 0, 1, or 2μM of methyl-β-cyclodextrin for 1h at 37℃, respectively. After 1 hour, the cells were treated with 2μM of HSA-Cu(Bp44mT) for another 4h at 37℃. The cells were then harvested in lysis buffer. After sonication, the samples were centrifuged for 20 min at 13,000 g. The protein concentration of the supernatant was determined by BCA (Beyotime Institute of Biotechnology, China) assay. The presence of Fe in the mice tumors was determined using inductively coupled plasma atomic emission spectrometry (ICP-AES). Sodium dodecyl sulfate–polyacrylamide gel electrophoresis was performed by loading equal amount of proteins per lane. Gels were then transferred to poly (vinylidene difluoride) membranes (Millipore) and blocked with 5% non-fat milk in TBST (20 mM Tris-HCl, 150 mM NaCl, and 0.05% Tween 20, pH 8.0) buffer for 1 h. The membranes were incubated with primary antibodies at 1:5000, diluted in 5% non−fat milk overnight at 4℃, and, after being washed four times with TBST for a total of 30 min, the secondary antibodies were conjugated with horseradish peroxidase at 1:5000 dilution for 1 h at room temperature and washed four times with TBST. The blots were visualized with the Amersham ECL

Plus Western blotting detection reagents according to the manufacturer's instructions. The membranes were stripped to detect the β-actin in order to assess the presence of comparable amount of proteins in each lane.

Determining the potential anticancer mechanistic of compound 12/HSA-12 complex

Topoisomerase IIα Inhibition Assay. The human Topo IIα kit was purchased from TopoGEN and Topo IIα activity was measured by the pBR322 DNA relaxation assay following the protocol provided by the manufacturer. Briefly, 20μL of the reaction mixture was prepared, which contained 0.2μg (6μL) of supercoiled pBR322 plasmid DNA, varying amounts of the ferric complex (5 μL), relaxation buffer (4 μL containing 50 mM Tris-HCl (pH 8.0), 150 mM NaCl, 10 mM $MgCl_2$, 0.5 mM ATP, and 0.5 mM dithiothreitol), and 1 unit of Topo IIα (5μL). Reaction mixtures were incubated for 30 min in the kinetic experiments as indicated at 37℃. The reaction mixtures were quenched by adding the stopping buffer (5% sarkosyl, 0.125% bromophenol blue, and 25% glycerol) and loaded on a 1% agarose gel in TBE buffer (45 mM Tris base, 45 mM boric acid, and 1 mM EDTA) and electrophoresed for 3 h at 80 V. The gel was then stained (1μg/mL) for 30 min and subsequently destained for 30 min (milli-Q water). The gels were photographed and analyzed using BioRad Gel Doc XR software. The Topo IIα inhibition percentage was obtained from the ratio of supercoiled DNA to the total DNA in each well. Nonhomogeneous backgrounds led to a large error of ±10% of the reported values in quantification.

Cell cycle distribution analysis. Bel-7402 cells were cultured in 70 mm culture

dishes, grown to 70% confluence, and treated with a determined concentration of compound **12** (1 μM) or HSA-**12** complex (1 μM). FACS analysis was performed after 24 h of treatment as described. To prepare for cell cycle analysis, the washed cells were fixed with 75% ethanol, washed with PBS, stained with PI, and then analyzed by flow cytometry using a 488 nm laser (FACScan, Becton Dickinson, San Jose, CA). For each sample, 10,000 events were recorded.

Intracellular reactive oxygen species (ROS) measurements. Intracellular ROS generation was determined using 2', 7'-dichlorodihydro-fluorescein diacetate (H_2DCF-DA) (Beyotime Institute of Biotechnology, Haimen, China). Bel-7402 cells (1×10^5 cells/well) were incubated with 1 μM of compound **6**, compound **12**, HSA-**12** complex, or $FeCl_3$ for 24 h at 37℃. Cells were then collected for flow cytometric assessment. The fluorescence intensity was monitored with excitation wavelength at 488 nm and emission wavelength at 525 nm.

Cyclic voltammetry. Cyclic voltammetry was performed with a BAS100B/W potentiostat. A glassy carbon working electrode, an aqueous Ag/AgCl reference electrode, and a Pt wire auxiliary electrode were used. All complexes were at ~ 1 mMin MeCN/H_2O (7:3 v/v); this solvent combination was used to ensure the solubility of all compounds. The supporting electrolyte was Et_4NClO_4 (0.1 M), and the solutions were purged with nitrogen prior to measurement. All potentials are cited versus the normal hydrogen electrode (NHE) by adding 196 mV to the potentials measured relative to the Ag/AgCl reference.

Change of mitochondrial membrane potential assay. Mitochondrial membrane

potential was analyzed with a fluorescent dye JC-1 (Beyotime Jiangsu China). Bel-7402 cells were treated with 1 μM of compound **6**, compound **12**, HSA-**12** complex, or $FeCl_3$ in 6-well plates and PBS was used as a control. Cells were then harvested after 24 h of incubation and stained with 1 mL of JC-1 (10 μg/mL) stock solution. Assays were initiated by incubating BeL-7402 cells with JC-1 for 20 min at 37℃ in the dark and the fluorescence of separated cells was detected with a flow cytometer (FACScan, Bection Dickinson, San Jose, CA).

Western blot analysis. BEL-7404 cells were seeded in 10 cm dishes for 24 h and incubated with 5 μM of compound **12** and HSA-**12** complex in the presence of 10% FBS. Cells were then harvested in lysis buffer. After sonication, the samples were centrifuged for 20 min at 13,000 g. The protein concentration of the supernatant was determined by BCA (Beyotime Institute of Biotechnology, China) assay. Sodium dodecyl sulfate–polyacrylamide gel electrophoresis was performed by loading equal amount of proteins per lane. Gels were then transferred to poly (vinylidene difluoride) membranes (Millipore) and blocked with 5% non-fat milk in TBST (20 mM Tris-HCl, 150 mM NaCl, and 0.05% Tween 20, pH 8.0) buffer for 1 h. The membranes were then incubated with primary antibodies at a dilution rate of 1:5000 in 5% non−fat milk overnight at 4℃. After being washed four times with TBST for a total of 30 min, the secondary antibodies were conjugated with horseradish peroxidase at a dilution rate of 1:5000 for 1 h at room temperature and then washed four times with TBST. The blots were visualized with Amersham's ECL Plus Western blotting detection reagents according to the manufacturer's instructions. To determine the presence of

comparable amount of proteins in each lane, the membranes were stripped to detect the β-actin.

Apoptosis by flow cytometry. The apoptotic events induced by compound **12** (1 μM) or HSA-**12** complex (1 μM) were determined with annexin V staining and PI according to the manufacturer's protocol for the Annexin V-FITC Apoptosis Detection Kit (Abcam). For these analyses, we used 1×10^5 cells/mL, which were incubated at 5% CO_2 and 37℃with the compound **12** (1 μM) or HSA-**12** complex (1 μM) for 12 h. The BeL-7402 cells were resuspended in 100 μL 1 × annexin V-binding buffer (10 mM Hepes/NaOH, 140 mM NaCl, and 2.5 mM $CaCl_2$, pH 7.4), and 5 μL each of annexin V and PI were added to each sample. Next, we incubated the cells for 15 min at room temperature and then subjected them to flow cytometric analysis (FACScan, Bection Dickinson, San Jose, CA). The rate of cell apoptosis was then analyzed.

Statistical analysis. All experiments were repeated between 3-5 times. Student's test was applied to evaluate the significance of the differences that were measured. Results are expressed as mean ± SD and considered to be significant when $P < 0.05$.

Ancillary Information

Supporting Information:

Determination of binding affinity of HSA for Fe compounds, Matrix-Assisted Laser Desorption Ionization Time-of-Flight Mass Spectrometry (MALDI-TOF-MS) Analyses, Crystal data for Fe compounds and Selected bond lengths (Å) and angles (deg) for Fe compounds.

PDB ID:

5GIX: HSA-PA-**12** complex.

Authors will release the atomic coordinates an experimental data upon article publication.

Corresponding Author:

Feng Yang

Email : fyang@mailbox.gxnu.edu.cn

Address: 9 Seyuan Road, Nantong, Jiangsu, China.

Zip code: 226019

Phone/Fax : 86-773-584-8836

Wei Zhang

Email : zhangw@ntu.edu.cn

Address: 9 Seyuan Road, Nantong, Jiangsu, China.

Zip code: 226019

Tao Wang

Email : wangtao@sustc.edu.cn

Address: 1088 Xueyuan Rd, Nanshan District, Shenzhen, Guangdong, China,

Zip code: 518055

ACKNOWLEDGMENTS

We are grateful to staff of Shanghai Synchrotron Radiation Facility for their technical assistance in data collection. This work was supported by the Natural Science Foundation of China (31460232, 31300600), the Natural Science Foundation of Guangxi (2014GXNSFDA118016), the National Key Basic Research Program of China (2013CB911501).

ABBREVIATIONS USED

BPS, bathophenanthrolinedisulfonate; DMSO, dimethylsulfoxide; DFO,

desferrioxamine; 3-AP, 3-aminopyridine-2-carboxaldehyde thiosemicarbazone; 311, 2-Hydroxy-1-naphthaldehyde isoniazid; SD, standard deviation; PI, propidium iodide.

REFERENCES

(1) Lainé, A.L.; Passirani, C. Novel metal-based anticancer drugs: a new challenge in drug delivery. *Curr. Opin. Pharmacol.* **2012**, *12*, 420-426.

(2) Yang, F.; Liang, H. HSA IIA subdomain-based developing anticancer metal prodrug: a new and improved approach. *Future Med. Chem.* **2016**, *8*, 89-91.

(3) Jansson, P. J.; Sharpe, P. C.; Bernhardt, P. V.; Richardson, D. R. Novel Thiosemicarbazones of the ApT and DpT series and their copper complexes: identification of pronounced redox activity and characterization of their antitumor activity. *J. Med. Chem*. **2010**, *53*, 5759–5769.

(4) Qi, J.; Liang, S.; Gou, Y.; Zhang, Z.; Zhou, Z.; Yang, F.; Liang, H. Synthesis of four binuclear copper(II) complexes: structure, anticancer properties and anticancer mechanism. *Eur. J. Med. Chem*. **2015**, *96*, 360-368.

(5) van Rijt, S. H.; Sadler, P. J. Current applications and future potential for bioinorganic chemistry in the development of anticancer drugs. *Drug Discov. Today*. **2009**, *14*,1089-1097.

(6) Kowol, C. R.; Trondl, R.; Heffeter, P.; Arion, V. B.; Jakupec, M. A.; Roller, A.; Galanski, M.; Berger, W.; Keppler, B. K. Impact of metal coordination on cytotoxicity of 3-aminopyridine-2-carboxaldehyde thiosemicarbazone (triapine) and novel insights into terminal dimethylation. *J. Med. Chem*. **2009**, *52*, 5032-5043.

(7) Lainé, A. L.; Passirani, C. Novel metal-based anticancer drugs: a new challenge

in drug delivery. *Curr. Opin. Pharmacol.* **2012**, *12*, 420-426.

(8) Whitnall, M.; Howard, J.; Ponka, P.; Richardson, D. R. A class of iron chelators with a wide spectrum of potent antitumor activity that overcomes resistance to chemotherapeutics. *Proc. Natl. Acad. Sci. U. S. A.* **2006**, 103, 14901-14906.

(9) Lovejoy, D.B.; Jansson, P.J.; Brunk, U.T.; Wong, J.; Ponka, P.; Richardson, D.R. Antitumor activity of metal-chelating compound Dp44mT is mediated by formation of a redox-active copper complex that accumulates in lysosomes. *Cancer Res.* **2011**, *71*, 5871-5880.

(10) Kalinowski, D. S.; Richardson, D. R. The evolution of iron chelators for the treatment of iron overload disease and cancer. *Pharmacol. Rev.* **2005**, *57*, 547–583.

(11) Ma, B.; Goh, B. C.; Tan, E. H.; Lam, K. C.; Soo, R.; Leong, S. S.; Wang, L. Z.; Mo, F.; Chan, A. T. C.; Zee, B.; Mok, T. A multicenter phase II trial of 3-aminopyridine-2-carboxaldehyde thiosemicarbazone (3-AP, Triapine (R)) and gemcitabine in advanced non-small-cell lung cancer with pharmacokinetic evaluation using peripheral blood mononuclear cells. *Invest. New Drugs.* **2008**, *26*, 169–173.

(12) Lovejoy, D. B.; Sharp, D. M.; Seebacher, N.; Obeidy, P.; Prichard, T.; Stefani, C.; Basha, M. T.; Sharpe, P. C.; Jansson, P. J.; Kalinowski, D. S.; Bernhardt, P. V.; Richardson, D. R. Novel second-generation di-2-pyridylketone thiosemicarbazones show synergism with standard chemotherapeutics and demonstrate potent activity against lung cancer xenografts after oral and intravenous administration in vivo. *J. Med. Chem.* **2012**, *55*, 7230-7244.

(13) Knox, J. J.; Hotte, S. J.; Kollmannsberger, C.; Winquist, E.; Fisher, B.;

Eisenhauer, E. A. Phase II study of triapine in patients with metastatic renal cell carcinoma: a trial of the national cancer institute of Canada clinical trials group (NCIC IND.161). *Invest. New Drugs.* **2007**, *25*, 471−477.

(14) Ma, B.; Goh, B. C.; Tan, E. H.; Lam, K. C.; Soo, R.; Leong, S. S.; Wang, L. Z.; Mo, F.; Chan, A. T.; Zee, B.; Mok, T. A Multicenter phase II trial of 3-aminopyridine-2-carboxaldehyde thiosemicarbazone (3-AP, Triapine) and gemcitabine in advanced non-small-cell lung cancer with pharmacokinetic evaluation using peripheral blood mononuclear cells. *Invest. New Drugs.* **2008**, *26*, 169−173.

(15) Yu, Y.; Kalinowski, D. S.; Kovacevic, Z.; Siafakas, A. R.; Jansson, P. J.; Stefani, C.; Lovejoy, D. B.; Sharpe, P. C.; Bernhardt, P. V.; Richardson, D. R. Thiosemicarbazones from the old to new: Iron chelators that are more than just ribonucleotide reductase inhibitors. *J. Med. Chem.* **2009**, *52*, 5271–5294.

(16) Richardson, D. R. Molecular mechanisms of iron uptake by cells and the use of iron chelators for the treatment of cancer. *Curr. Med. Chem.* **2005**, *12*, 2711–2729.

(17) Liu, F.; Mu, J.; Xing, B. Recent advances on the development of pharmacotherapeutic agents on the basis of human serum albumin. *Curr. Pharm. Des.* **2015**, *21*, 1866-1888.

(18) Fanali, G.; di Masi, A.; Trezza, V.; Marino, M.; Fasano, M.; Ascenzi, P. Human serum albumin: from bench to bedside. *Mol. Aspects Med.* **2012**, *33*, 209-90.

(19) Peters, T. All about albumin: biochemistry, genetics, and medical applications. *Academic Press, San Diego. 1996*.

(20) Ghuman, J.; Zunszain, P. A.; Petitpas, I.; Bhattacharya, A. A.; Otagiri, M.; Curry,

S. Structural basis of the drug-binding specificity of human serum albumin. *J. Mol. Biol.* **2005**, *353*, 38-52.

(21) Zsila, F. Subdomain IB is the third major drug binding region of human serum albumin: toward the three-sites model. *Mol. Pharm.* **2013**, *10*, 1668-1682.

(22) Lambrinidis, G.; Vallianatou, T.; Tsantili-Kakoulidou, A. In vitro, in silico and integrated strategies for the estimation of plasma protein binding. A review. *Adv. Drug Deliv. Rev*. **2015**, 86, 27-45.

(23) Kragh-Hansen, U. Molecular and practical aspects of the enzymatic properties of human serum albumin and of albumin-ligand complexes. *Biochim. Biophys. Acta*. **2013**, *1830*, 5535-5544.

(24) He, X. M.; Carter, D. C. Atomic structure and chemistry of human serum albumin. *Nature.* **1992**, *358*, 209–215.

(25) Zhang, Y.; Ho, A.; Yue, J.; Kong, L.; Zhou, Z.; Wu, X.; Yang, F.; Liang, H. Structural basis and anticancer properties of ruthenium-based drug complexed with human serum albumin. *Eur. J. Med. Chem.* **2014**, *86*, 449-455.

(26) Gou, Y.; Qi, J.; Ajayi, J.P.; Zhang, Y.; Zhou, Z.; Yang, F.; Liang, H. Developing anticancer copper(II) pro-drugs based on the nature of cancer cells and the human serum albumin carrier IIA subdomain. *Mol. Pharm.* **2015**, *12*, 3597-3609.

(27) Durante, S.; Orienti, I.; Teti, G.; Salvatore, V.; Focaroli, S.; Tesei, A.; Pignatta, S.; Falconi, M. Anti-tumor activity of fenretinide complexed with human serum albumin in lung cancer xenograft mouse model. *Oncotarget*. **2014**, *5*, 4811-4820.

(28) Sasson, K.; Marcus, Y.; Lev-Goldman, V.; Rubinraut, S.; Fridkin, M.; Shechter,

Y. Engineering prolonged-acting prodrugs employing an albumin-binding probe that undergoes slow hydrolysis at physiological conditions. *J. Control Release*. **2010**, *142*, 214-220.

(29) Kratz, F. Albumin as a drug carrier: design of prodrugs, drug conjugates and nanoparticles. *J. Control Release.* **2008**, *132*, 171-183.

(30) Gou, Y.; Yang, F.; Liang, H. Designing prodrugs based on special residues of human serum albumin. *Curr. Top Med. Chem*. **2016**, 16, 996-1008.

(31) Elsadek, B.; Kratz, F. Impact of albumin on drug delivery—New applications on the horizon. *J. Control. Release.* **2012**, *157*, 4-28.

(32) Zhang, Y.; Ho, A.; Yue, J.; Kong, L.; Zhou, Z.; Wu, X.; Yang, F.; Liang, H. Structural basis and anticancer properties of ruthenium-based drug complexed with human serum albumin. *Eur. J. Med. Chem.* **2014**, *86*, 449-455.

(33) Gou, Y.; Qi, J.; Ajayi, J.P.; Zhang, Y.; Zhou, Z.; Yang, F.; Liang, H. Developing anticancer copper(II) pro-drugs based on the nature of cancer cells and the human serum albumin carrier IIA subdomain. *Mol. Pharm.* **2015**, *12*, 3597-3609.

(34) Qi, J.; Zhang, Y.; Gou, Y.; Zhang, Z.; Zhou, Z.; Wu, X.; Yang, F.; Liang, H. Developing an anticancer copper(II) pro-drug based on the His242 residue of the human serum albumin carrier IIA subdomain. *Mol. Pharm.* **2016**, *13*, 1501-1507.

(35) Torre, L. A.; Bray, F.; Siegel, R. L.; Ferlay, J.; Lortet-Tieulent, J.; Jemal, A. Global cancer statistics, 2012. *CA. Cancer J. Clin*. **2015**, *65*, 87-108.

(36) Lovejoy, D. B.; Richardson, D. R. Novel "hybrid" iron chelators derived from aroylhydrazones and thiosemicarbazones demonstrate selective antiproliferative

activity against tumor cells. *Blood*. **2002**, *100*, 666-676.

(37) Ferraro, G.; Massai, L.; Messori, L.; Merlino, A. Cisplatin binding to human serum albumin: a structural study. *Chem. Commun.* **2015**, *51*, 9436-9439.

(38) Desai, N. Nab Technology: A drug delivery platform utilizing endothelial gp60 receptor-based transport and tumor derived SPARC for targeting. *Drug Delivery Report Winter 2007/008*, **2007**.

(39) Atorrasagasti, C.; Malvicini, M.; Aquino, J.B.; Alaniz, L.; Garcia, M.; Bolontrade, M; Rizzo, M.; Podhajcer, O.L.; Mazzolini, G. Overexpression of SPARC obliterates the in vivo tumorigenicity of human hepatocellular carcinoma cells. *Int. J. Cancer*. **2010**, *126*, 2726-2740.

(40) Tiruppathi, C.; Naqvi, T.; Wu, Y.; Vogel, S.M.; Minshall, R.D.; Malik, A.B. Albumin mediates the transcytosis of myeloperoxidase by means of caveolae in endothelial cells. *Proc. Natl. Acad. Sci. U. S. A*. **2004**, *101*, 7699-7704.

(41) Larsen, A. K.; Escargueil, A. E.; Skladanowski, A. Catalytic topoisomerase II inhibitors in cancer therapy. *Pharmacol. Ther*. **2003**, *99,* 167–181.

(42) Zeglis, B. M.; Divilov, V.; Lewis, J. S. Role of metalation in the topoisomerase IIα inhibition and antiproliferation activity of a series of α-heterocyclic-N4-substituted thiosemicarbazones and their Cu(II) complexes. *J. Med .Chem.* **2011**, *54*, 2391-2398.

(43) Miller, M. C.; Bastow, K. F.; Stineman, C. N.; Vance, J. R.; Song, S. C.; West, D. X.; Hall, I. H. The cytotoxicity of 2-formyl and 2-acetyl-(6-picolyl)-4N-substituted thiosemicarbazones and their copper(II) complexes. *Arch. Pharm.* **1998**, *331*,

121–127.

(44) Huang, H.; Chen, W.; Ku, X.; Meng, L.; Lin, L.; Wang, X.; Zhu, C.; Wang, Y.; Chen, Z.; Li, M.; Jiang, H.; Chen, K.; Ding, J.; Liu, H. A series of alpha-heterocyclic carboxaldehyde thiosemicarbazones inhibit topoisomerase-II catalytic activity. *J. Med. Chem.* **2010**, *53*, 3048–3064.

(45) Rao, V. A.; Klein, S. R.; Agama, K. K.; Toyoda, E.; Adachi, N.; Pommier, Y.; Shacter, E. B. The iron chelator Dp44mT causes DNA damage and selective inhibition of topoisomerase-II in breast cancer cells. *Cancer Res.* **2009**, *69*, 948–957.

(46) Eastman, A. Cell cycle checkpoints and their impact on anticancer therapeutic strategies. *J. Cell Biochem.* **2004**, *91*, 223-231.

(47) Masai, H.; Matsumoto, S.; You, Z.; Yoshizawa-Sugata, N.; Oda, M. Eukaryotic chromosome DNA replication: where, when, and how? *Annu. Rev. Biochem*. **2010**, *79*, 89-130.

(48) Kang, K.; Nho, C. W.; Kim, N. D.; Song, D, G.; Park, Y. G.; Kim, M.; Pan, C. H.; Shin, D.; Oh, S. H.; Oh, H. S. Daurinol, a catalytic inhibitor of topoisomerase IIα, suppresses SNU-840 ovarian cancer cell proliferation through cell cycle arrest in S phase. *Int. J. Oncol*. **2014**, *45*, 558-566.

(49) Stefani, C.; Jansson, P. J.; Gutierrez, E.; Bernhardt, P. V.; Richardson, D. R.; Kalinowski, D. S. Alkyl substituted 2'-benzoylpyridine thiosemicarbazone chelators with potent and selective anti-neoplastic activity: novel ligands that limit methemoglobin formation. *J. Med. Chem*. **2013**, *56*, 357-370.

(50) Jiang, G. B.; Zheng, X.; Yao, J. H.; Han, B. J.; Li, W.; Wang, J.; Huang, H. L.;

Liu, Y. J. Ruthenium(II) polypyridyl complexes induce BEL-7402 cell apoptosis by ROS-mediated mitochondrial pathway. *J. Inorg. Biochem.* **2014**, *141*, 170-179.

(51) Trachootham, D.; Alexandre, J.; Huang, P. Targeting cancer cells by ROS-mediated mechanisms: a radical therapeutic approach? *Nat. Rev. Drug Discov.* **2009**, *8*, 579-591.

(52) Han, C. R.; Jun do, Y.; Kim, Y. H.; Lee, J. Y.; Kim, Y. H. Prometaphase arrest-dependent phosphorylation of Bcl-2 family proteins and activation of mitochondrial apoptotic pathway are associated with 17α-estradiol-induced apoptosis in human Jurkat T cells. *Biochim. Biophys. Acta.* **2013**, *1833*, 2220-2232.

(53) He, L.; Liao, S. Y.; Tan, C. P.; Ye, R. R.; Xu, Y. W.; Zhao, M.; Ji, L. N.; Mao, Z. W. Ruthenium-Arene-β-Carboline complexes as potent inhibitors of cyclin-dependent kinase 1: synthesis, characterization and anticancer mechanism studies. *Chemistry*. **2013**, *19*, 12152-12160.

(54) Marzec, K. A.; Lin, M. Z.; Martin, J. L.; Baxter, R. C. Involvement of p53 in insulin-like growth factor binding protein-3 regulation in the breast cancer cell response to DNA damage. *Oncotarget*. **2015**, *6*, 26583-26598.

(55) Sheldrick, G. M. SHELXTL V5.1: software reference manual, bruker AXS. *Inc., Madison, WI, U. S. A*. **1997**.

(56) Curry, S.; Mandelkow, H.; Brick, P.; Franks, N. Crystal structure of human serum albumin complexed with fatty acid reveals an asymmetric distribution of binding sites. *Nat. Struct. Biol*. **1998**, *5*, 827–835.

(57) Otwinowski, Z.; Minor, W. Processing of X-ray diffraction data collected in

oscillation mode. *Methods Enzymol*. **1997**, *276*, 307-326.

(58) Adams, P.D.; Afonine, P.V.; Bunkóczi, G.; Chen, V.B.; Davis, I.W.; Echols, N.; Headd, J.J.; Hung, L.W.; Kapral, G.J.; Grosse-Kunstleve, R.W.; McCoy, A.J.; Moriarty, N.W.; Oeffner, R.; Read, R.J.; Richardson, D.C.; Richardson, J.S.; Terwilliger, T.C.; Zwart, P.H. PHENIX: a comprehensive Python-based system for macromolecular structure solution. *Acta. Crystallogr. D Biol. Crystallogr*. **2010**, *66*, 213-221.

(59) Emsley, P.; Cowtan, K. Coot: model-building tools for molecular graphics. *Acta. Crystallogr. D Biol. Crystallogr*. **2004**, *60*, 2126-2132.

(60) DeLano, W. L. The PyMol molecular graphics system. *DeLano ScientiWc, San Carlos*, *CA*. **2004**.

(61) Du, C.; Deng, D.; Shan, L.; Wan, S.; Cao, J.; Tian, J.; Achilefu, S.; Gu, Y. A pH-sensitive doxorubicin prodrug based on folate-conjugated BSA for tumor-targeted drug delivery. *Biomaterials*. **2013**, 34, 3087−3097.

Table 1 IC_{50} values of compounds and HSA complexes toward cell lines for 48 h.

	IC_{50} (μM)	
	Bel-7402	HL-7702
compound **1**	> 40	> 40
compound **2**	> 40	> 40
compound **3**	> 40	> 40
compound **4**	> 40	> 40
compound **5**	> 40	> 40
compound **6**	> 40	> 40
compound **7**	13.36 ± 1.35	15.32 ± 0.85
compound **8**	11.87 ± 1.25	11.24 ± 0.65
compound **9**	2.22 ± 0.66	3.33 ± 0.39
compound **10**	0.86 ± 0.23	0.95 ± 0.28
compound **11**	0.92 ± 0.37	0.99 ± 0.31
compound **12**	0.65 ± 0.25	0.78 ± 0.15
HSA-**7** complex	8.37 ± 1.56	17.33 ± 1.66
HSA-**8** complex	5.21 ± 0.55	16.35 ± 1.12
HSA-**9** complex	0.96 ± 0.11	4.25 ± 0.85
HSA-**10** complex	0.34 ± 0.06	3.24 ± 0.37
HSA-**11** complex	0.37 ± 0.06	3.96 ± 0.09
HSA-**12** complex	0.11 ± 0.03	3.56 ± 0.28
Cis-platin	14.54 ± 0.85	15.62 ± 0.63
HSA	> 100	> 100
$FeCl_3$	> 60	> 60

Table 2 Serological analysis of mice injected NaCl, compound 12 and HSA-12 complex.

Complex	CK (U/L)	BUN (mmol/L)	ALT (U/L)	AST (U/L)
NaCl	316 ± 12	8.1 ± 1.2	32.2 ± 8.6	82.5 ± 17
compound **12**	352 ± 25	25.0 ± 2.1	55.5 ± 5.9	125 ± 18
HSA-**12** complex	323 ± 26	7.6 ± 1.5	36.6 ± 6.0	90 ± 7.8

Table 3 Data collection and refinement statistics of HSA complex

	HSA-PA-**12**
Data collection	
Space group	P1
Cell dimensions□□	
a, *b*, *c* (Å)	38.47, 94.55, 96.11
α□□β□□γ(°)	104.90, 89.90, 100.86
Wavelength(Å)	1.0
Resolution (Å)	27.13-2.80 (2.90-2.80)
R_{merge}	6.9% (24.1%)
$I/\sigma I$	13.6 (4.3)
Completeness (%)	96% (96.8%)
Redundancy	4.2
Refinement	
Resolution (Å)	27.13-2.80
No. reflections	30491(2968)
R_{work} / R_{free}	0.209/0.267
No. of Non-H atoms	9462
Protein	9212
Ligand	248
Average *B,* All atoms(Å^2)	66.41
Protein	66.30
Ligands	70.70
r.m.s. deviations	
Bond lengths (Å)	0.019
Bond angles (°)	1.33

[a] Values for the outermost resolution shell are given in parentheses.

[b] $R_{merge}=100\times\Sigma_h\Sigma_j|I_{hj}-I_h|/\Sigma_h\Sigma_j I_{hj}$ where I_h is the weighted mean intensity of the symmetry-related refractions I_{hj}.

[c] $R_{work}=100\times\Sigma_{hkl}|F_{obs}-F_{calc}|/\Sigma_{hkl}F_{obs}$ where F_{obs} and F_{calc} are the observed and calculated structure factors, respectively.

[d] R_{free} is the R_{work} calculated using a randomly selected 5% sample of reflection data omitted from the refinement.

FIGURE LEGENDS

Figure 1 The hypothesis of developing Fe pro-drug based on the N-donor residues of HSA IIA subdomain.

Figure 2 The structure of ligands and Fe compounds.

Figure 3 (A) Experimental sigmaA weighted 2Fo-Fc electron density map of compound **12** at IIA subdomain; (B) The overall structure of the HSA complex; (C) The structural binding environment of compound **12** to IIA subdomain of HSA. Amino acid chains that are close to the drug molecules are shown as sticks.

Figure 4 (A) Net tumor volume as a function of time on Bel-7402 xenografts after IV administration (tail vein) of vehicle control, compound **12** and HSA-**12** complex. (B) Tumor weight (wet weight) (A) after killing the mice on Day 28. (C) Tumors were removed from the mice after 28 days of treatment and stained with the TUNEL assay (400x).Results are mean ± SD (n = 6−7 mice/condition). Results are mean ± SD (n = 6−7): (*) $p < 0.05$ (**) $p < 0.01$, (***) $p < 0.001$.

Figure 5 (A) The average body weight of treated nude mice was measured and recorded for 28 days. (B) After 28 days of treatment, the major organs (heart, liver, and kidney) were harvested from mice and then stained with Hematoxylin and Eosin (400x).

Figure 6 (A) Fe content in tumor of mice treated with compound **12** and HSA-**12** complex after 28 days. (B) The Fe content released from HSA complex in pH 4.7, and 7.4 buffers, 0-48h, respectively.

Figure 7 (A) Western blot analysis of HSA in Bel-7402 cells treated with HSA-**12** complex; β-actin was used as the internal control. (B) Percentage levels of HSA; the

values are relative to 0 mM of methyl-β-cyclodextrin-incubated. (C) Intracellular Fe concentration in Bel-7402 cells treated with HSA-**12** complex relative to 0 mM of methyl-β-cyclodextrin-incubated.

Figure 8 (A) Agarose gel assay for Topo-IIα inhibition by compound **12**. (B) The effect of the cell cycle of Bel-7402 treated with compound **12** and HSA-**12** complex for 24 h compared with untreated cells. (C) Western blot analysis of E2F-1, Cyc A, Cyc E, and Cdk 2 in Bel-7402 cells treated with compound **12** and HSA-**12** complex for 24 h; β-actin was used as the internal control. (D) Expression levels of (C) in panel shown as percentages. The values are relative to the control.

Figure 9 (A) Intracellular production of reactive oxygen species by $FeCl_3$, compound **6**, compound **12** and HSA-**12** complex following a 24 h incubation determined by flow cytotometric. (B) Cyclic voltammograms of 1 mM solutions of compound **12** shows the impact of a halogen atom on the $Fe^{III/II}$ redox potential. (C) The percentage of green fluorescence cells treated with $FeCl_3$, compound **6**, compound **12** and HSA-**12** complex for 24 h and control determined by flow cytotometric.

Figure 10 (A) Western blot analysis of p53, Bcl-2, Bcl-xl, Bax, Cyt C, Caspase-3, and Caspase-9 in Bel-7402 cells treated with compound **12** and HSA-**12** complex for 24 h; β-actin was used as the internal control. (B) Expression levels of p53, Bcl-2, Bcl-xl, Bax, Cyt C, Caspase-3, and Caspase-9 shown as percentages; the values are relative to the control. (C) The effect of cell apoptosis from Bel-7402 treated with compound **12** and HSA-**12** complex for 12 h compared with the untreated cells.

Figure 11 The possible delivery and anticancer mechanism of HSA-**12** complex.

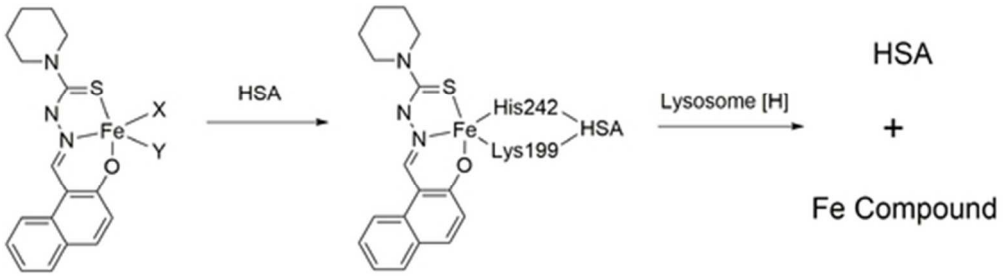

Figure 1 The hypothesis of developing Fe pro-drug based on the N-donor residues of HSA IIA subdomain.

46x12mm (300 x 300 DPI)

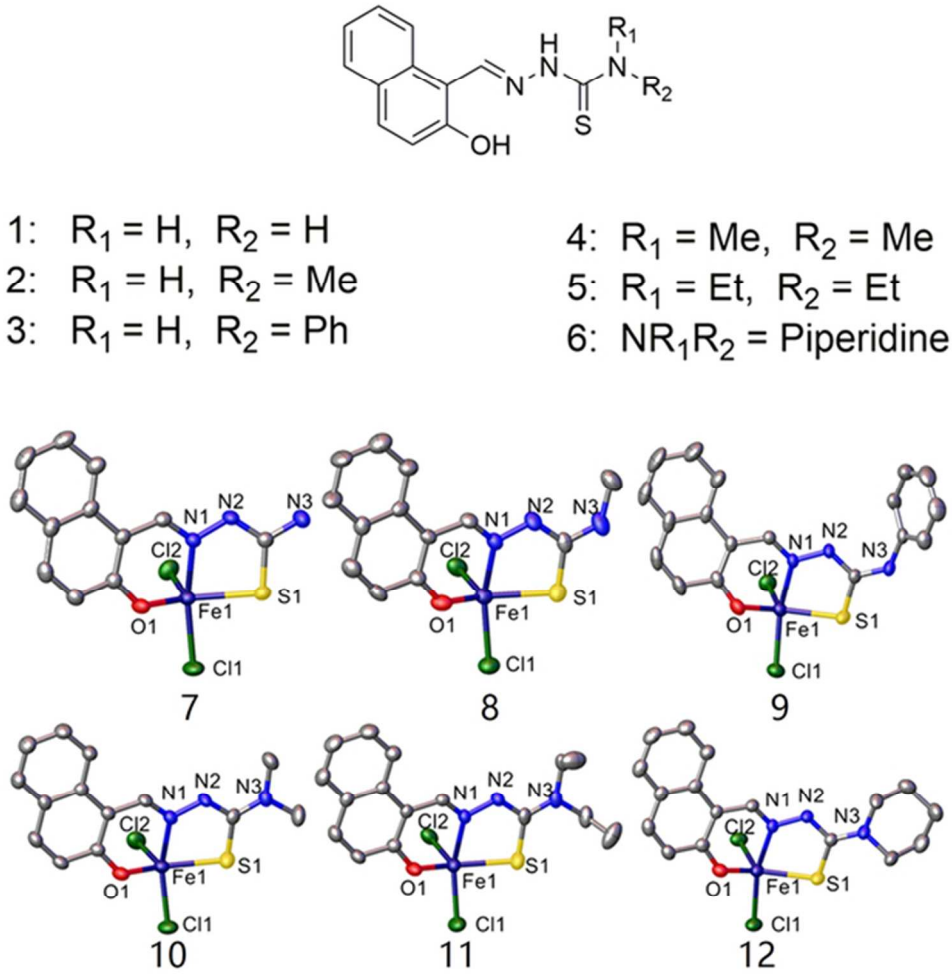

Figure 2 The structure of ligands and Fe compounds.

54x56mm (300 x 300 DPI)

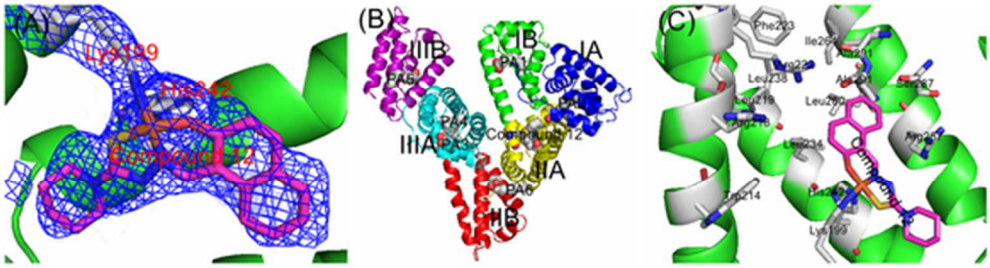

Figure 3 (A) Experimental sigmaA weighted 2Fo-Fc electron density map of compound 12 at IIA subdomain; (B) The overall structure of the HSA complex; (C) The structural binding environment of compound 12 to IIA subdomain of HSA. Amino acid chains that are close to the drug molecules are shown as sticks.

49x13mm (300 x 300 DPI)

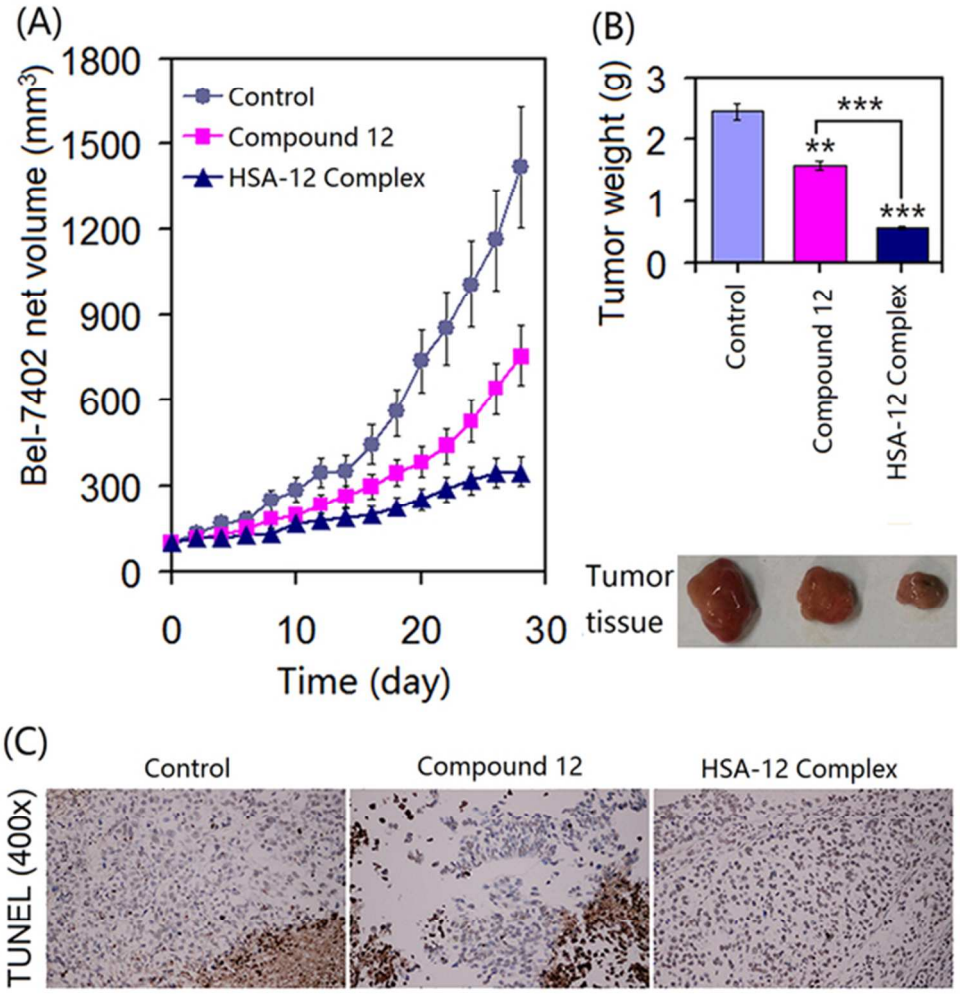

Figure 4 (A) Net tumor volume as a function of time on Bel-7402 xenografts after IV administration (tail vein) of vehicle control, compound 12 and HSA-12 complex. (B) Tumor weight (wet weight) (A) after killing the mice on Day 28. (C) Tumors were removed from the mice after 28 days of treatment and stained with the TUNEL assay (400x).Results are mean ± SD (n = 6−7 mice/condition). Results are mean ± SD (n = 6−7): (*) $p < 0.05$ (**) $p < 0.01$, (***) $p < 0.001$.

54x56mm (300 x 300 DPI)

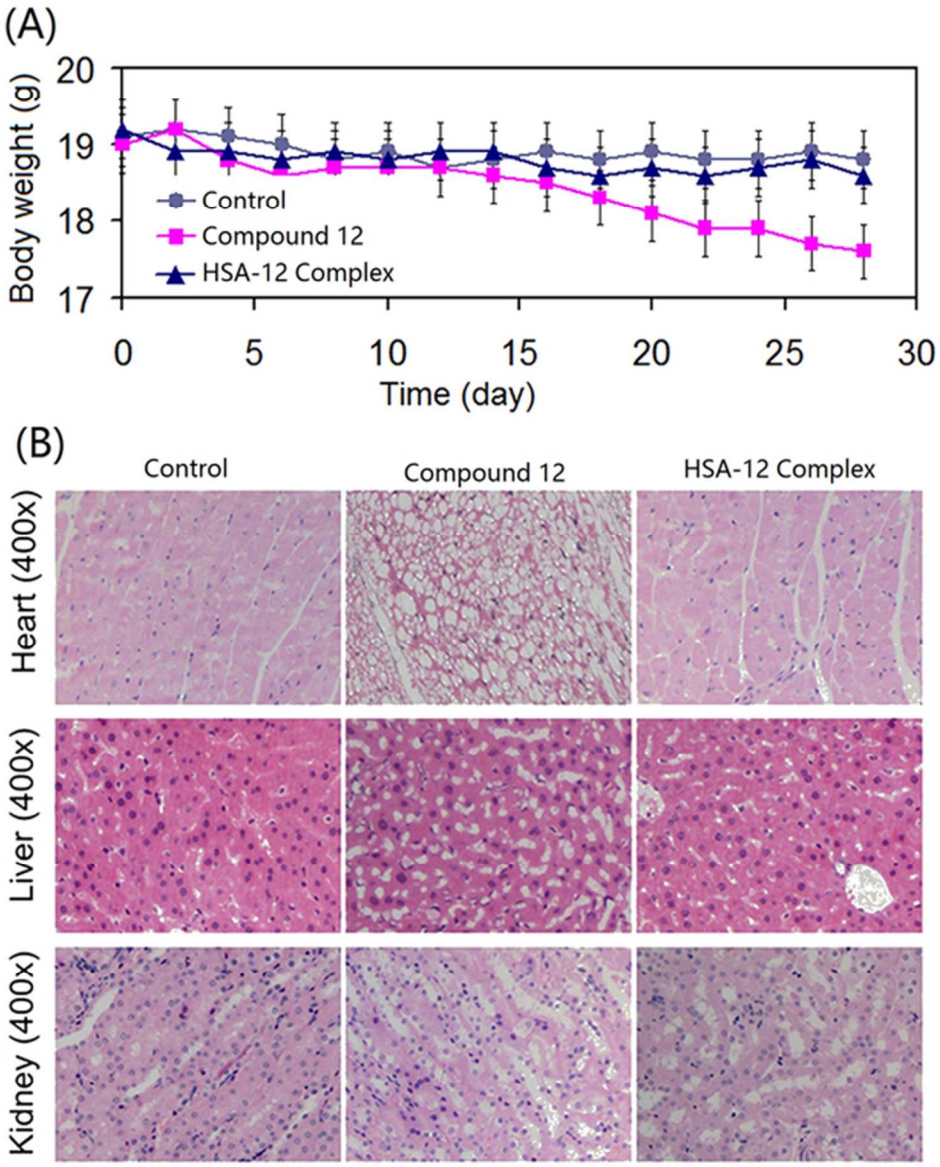

Figure 5 (A) The average body weight of treated nude mice was measured and recorded for 28 days. (B) After 28 days of treatment, the major organs (heart, liver, and kidney) were harvested from mice and then stained with Hematoxylin and Eosin (400x).

54x66mm (300 x 300 DPI)

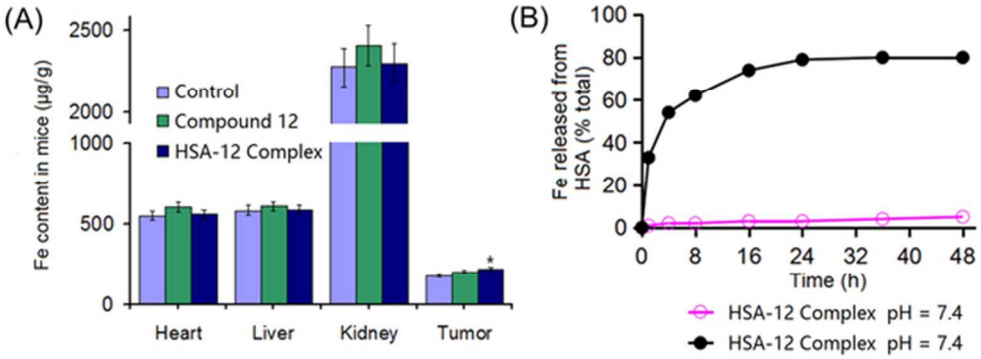

Figure 6 (A) Fe content in tumor of mice treated with compound 12 and HSA-12 complex after 28 days. (B) The Fe content released from HSA complex in pH 4.7, and 7.4 buffers, 0-48h, respectively.

54x19mm (300 x 300 DPI)

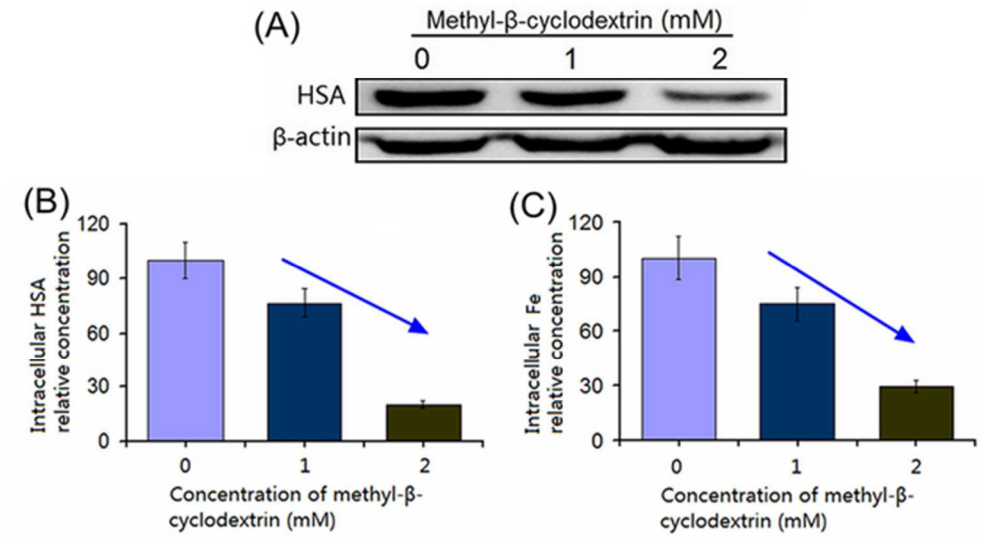

Figure 7 (A) Western blot analysis of HSA in Bel-7402 cells treated with HSA-12 complex; β-actin was used as the internal control. (B) Percentage levels of HSA; the values are relative to 0 mM of methyl-β-cyclodextrin-incubated. (C) Intracellular Fe concentration in Bel-7402 cells treated with HSA-12 complex relative to 0 mM of methyl-β-cyclodextrin-incubated.

54x30mm (300 x 300 DPI)

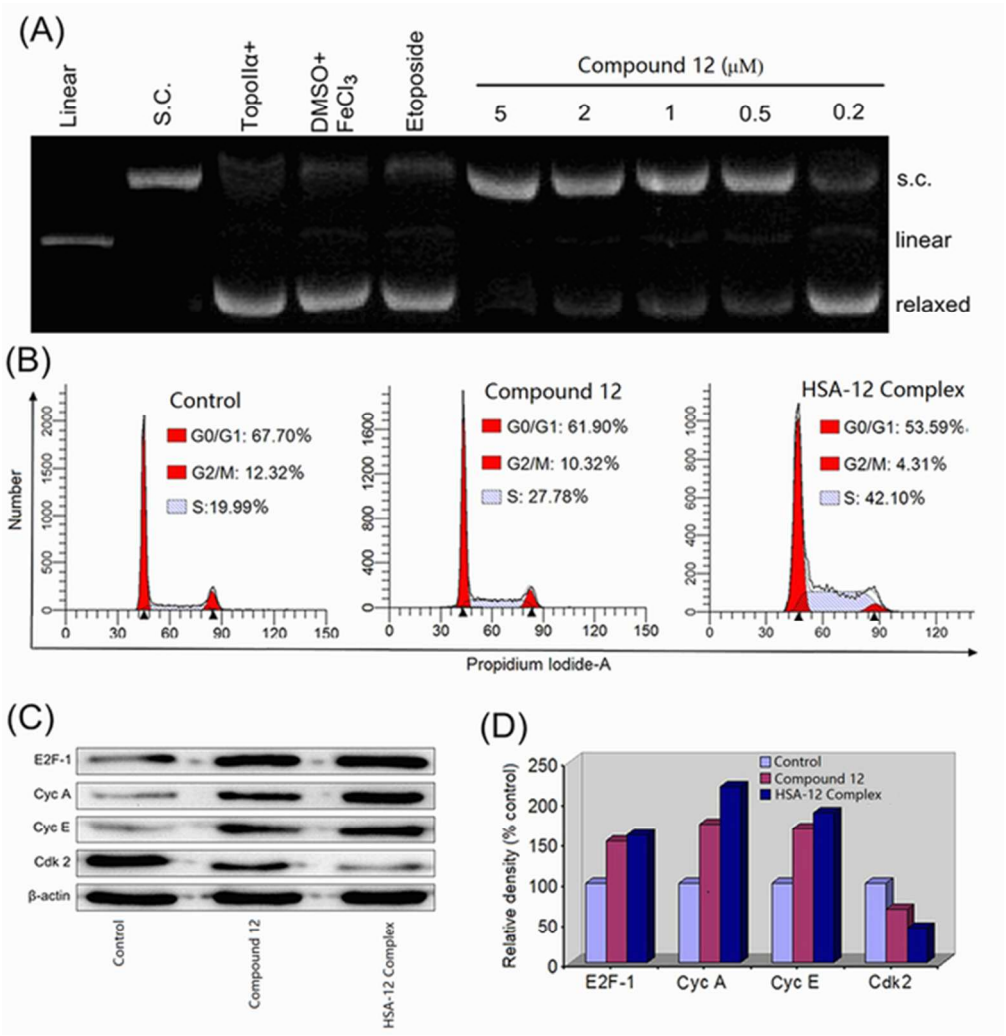

Figure 8 (A) Agarose gel assay for Topo-IIα inhibition by compound 12. (B) The effect of the cell cycle of Bel-7402 treated with compound 12 and HSA-12 complex for 24 h compared with untreated cells. (C) Western blot analysis of E2F-1, Cyc A, Cyc E, and Cdk 2 in Bel-7402 cells treated with compound 12 and HSA-12 complex for 24 h; β-actin was used as the internal control. (D) Expression levels of (C) in panel shown as percentages. The values are relative to the control.

54x55mm (300 x 300 DPI)

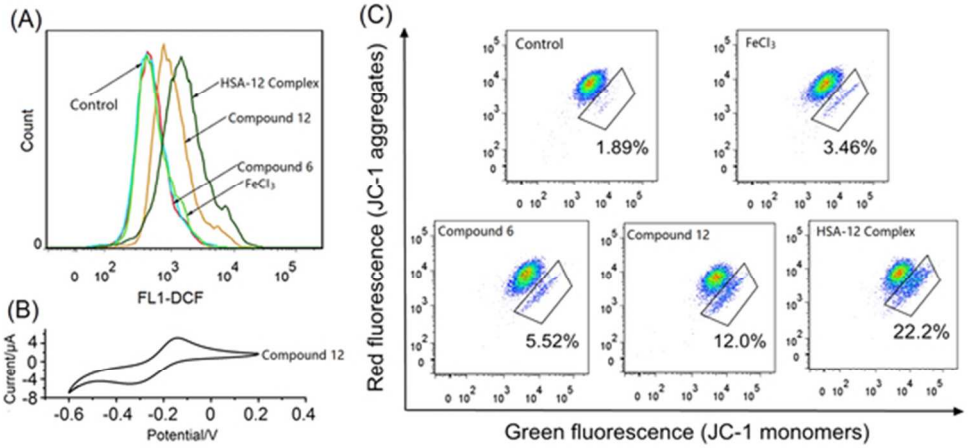

Figure 9 (A) Intracellular production of reactive oxygen species by FeCl3, compound 6, compound 12 and HSA-12 complex following a 24 h incubation determined by flow cytometric. (B) Cyclic voltammograms of 1 mM solutions of compound 12 shows the impact of a halogen atom on the FeIII/II redox potential. (C) The percentage of green fluorescence cells treated with FeCl3, compound 6, compound 12 and HSA-12 complex for 24 h and control determined by flow cytometric.

54x25mm (300 x 300 DPI)

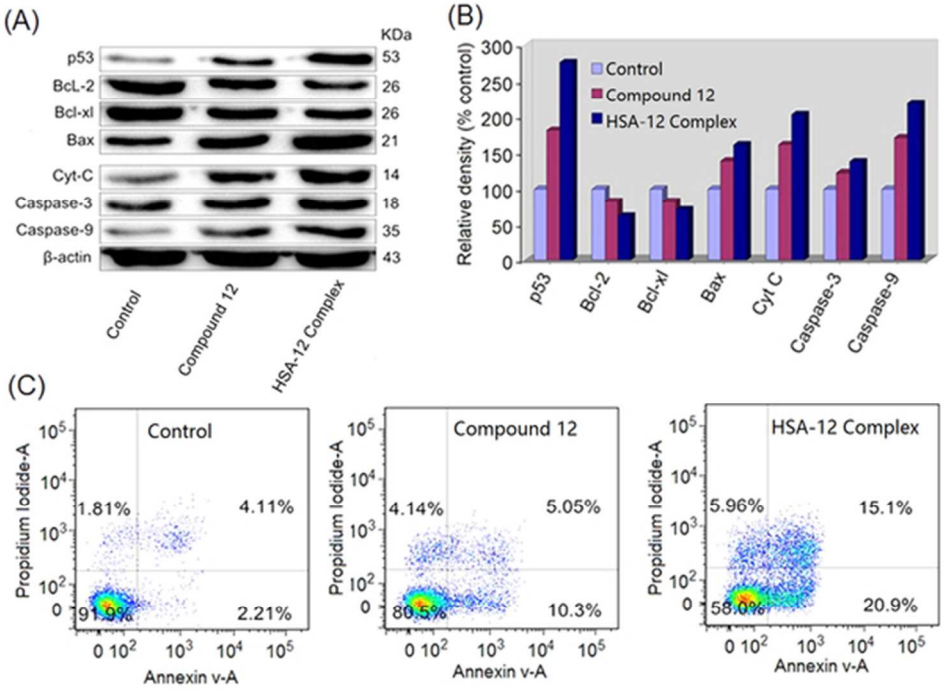

Figure 10 (A) Western blot analysis of p53, Bcl-2, Bcl-xl, Bax, Cyt C, Caspase-3, and Caspase-9 in Bel-7402 cells treated with compound 12 and HSA-12 complex for 24 h; β-actin was used as the internal control. (B) Expression levels of p53, Bcl-2, Bcl-xl, Bax, Cyt C, Caspase-3, and Caspase-9 shown as percentages; the values are relative to the control. (C) The effect of cell apoptosis from Bel-7402 treated with compound 12 and HSA-12 complex for 12 h compared with the untreated cells.

54x38mm (300 x 300 DPI)

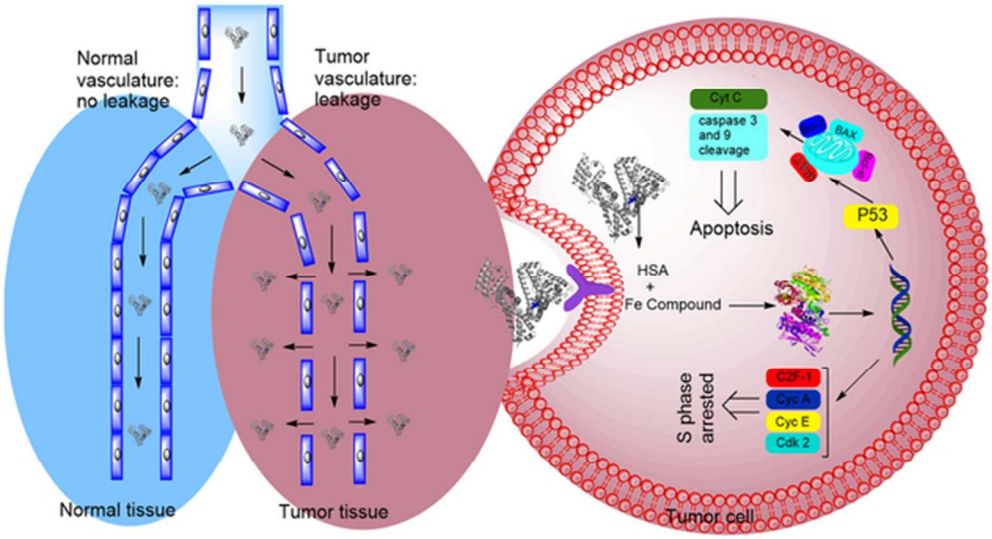

Figure 11 The possible delivery and anticancer mechanism of HSA-12 complex.

54x30mm (300 x 300 DPI)

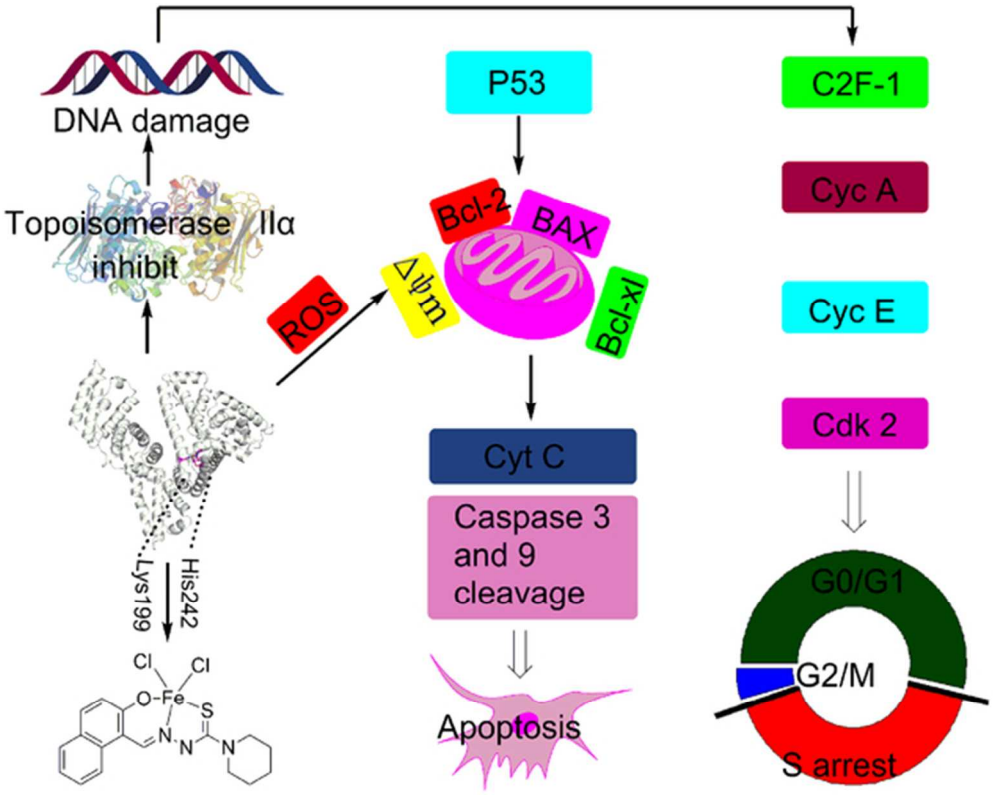

TABLE OF CONTENTS GRAPHIC

54x43mm (300 x 300 DPI)